CERN-EP-2022-174
12 August 2022

Multiplicity dependence of Υ production at forward rapidity in pp collisions at $\sqrt{s} = 13$ TeV

ALICE Collaboration*

Abstract

The measurement of $\Upsilon(1S)$, $\Upsilon(2S)$, and $\Upsilon(3S)$ yields as a function of the charged-particle multiplicity density, $dN_{ch}/d\eta$, using the ALICE experiment at the LHC, is reported in pp collisions at $\sqrt{s} = 13$ TeV. The Υ meson yields are measured at forward rapidity ($2.5 < y < 4$) in the dimuon decay channel, whereas the charged-particle multiplicity is defined at central rapidity ($|\eta| < 1$). Both quantities are divided by their average value in minimum bias events to compute the self-normalized quantities. The increase of the self-normalized $\Upsilon(1S)$, $\Upsilon(2S)$, and $\Upsilon(3S)$ yields is found to be compatible with a linear scaling with the self-normalized $dN_{ch}/d\eta$, within the uncertainties. The self-normalized yield ratios of excited-to-ground Υ states are compatible with unity within uncertainties. Similarly, the measured double ratio of the self-normalized $\Upsilon(1S)$ to the self-normalized J/ψ yields, both measured at forward rapidity, is compatible with unity for self-normalized charged-particle multiplicities beyond one. The measurements are compared with theoretical predictions incorporating initial or final state effects.

© 2022 CERN for the benefit of the ALICE Collaboration.

Reproduction of this article or parts of it is allowed as specified in the CC-BY-4.0 license.

*See Appendix C for the list of collaboration members

1 Introduction

At the Large Hadron Collider (LHC) energies, our understanding of hadronic collisions has been challenged by the observation that a large class of phenomena, traditionally associated with the presence of a deconfined medium, shows a smooth evolution from small colliding systems such as proton–proton (pp) and proton–lead (p–Pb) to large systems like lead–lead (Pb–Pb) [1, 2]. It is still actively debated whether these phenomena could be ascribed to the formation of a hot and dense medium (i.e. the quark–gluon plasma, QGP) in small systems, or to other collective effects or specific QCD processes at play in high charged-particle multiplicity events, possibly associated to a peculiar initial state of the collision.

Any attempt to build a coherent framework linking the observations from small to large collision systems must then include a proper characterization of the initial state of hadronic collisions, and of the mechanisms responsible for the existence of high charged-particle multiplicity density events. Here and in the rest of this paper, “charged-particle multiplicity density” is defined as the number of charged particles produced per unit of pseudorapidity η , where the pseudorapidity is defined as $\eta = -\ln \tan(\theta/2)$, θ being the polar angle of a particle momentum with respect to the beam axis. One such mechanism is the multiparton interaction (MPI), which allows the simultaneous occurrence of several incoherent binary partonic interactions in a single nucleon–nucleon collision [3]. MPIs play a significant role in describing the soft component of the hadronic interactions, as confirmed by the measured charged-particle multiplicity distributions in pp collisions at center-of-mass energies $\sqrt{s} = 0.9\text{--}8$ TeV [4]. Based on this, event generators such as PYTHIA 8 [5, 6] and EPOS [7] currently highlight the importance of MPIs in building the charged-particle multiplicity distributions in hadronic interactions [8].

The production of heavy flavour hadrons is usually computed in a factorization approach, where the perturbative treatment of the early-stage hard-parton scattering processes, described by perturbative QCD (pQCD), is followed by the subsequent, soft-scale, hadronization of the scattered partons resulting in their binding into color-neutral states. For the production of quarkonium states, charmonia or bottomonia, several descriptions are available for the hadronization stage (e.g. the color singlet and color octet ones) [9, 10]. Bottomonium states, such as the particles of the Υ family, are of particular interest as a probe of the QGP and are considered a tool to characterize the QGP properties. The interaction of the $\Upsilon(nS)$ states with the hot and dense medium is expected to result in a sequential dissociation of the states, with the more tightly bound ones being dissociated at higher temperatures [10–12]. The measurements in central heavy–ion collisions support this scenario, where the dissociation of the quarkonium states is partly compensated by the recombination of the bound states, expected to be more relevant for charmonium than for bottomonium states (see Refs.[13–24] and references therein). The results in proton–nucleus collisions evidence a suppression of J/ψ yields at forward (central) rapidity at the LHC (RHIC) energies, with respect to binary-collision-scaled yields pp collisions, described by several models, see Refs. [25–29]. The excited $\psi(2S)$ state presents a stronger suppression than J/ψ in proton–nucleus collisions at backward rapidity, suggesting a non-negligible influence of final-state effects [30–36]. In the bottomonium sector, there is an indication of $\Upsilon(nS)$ suppression in proton–nucleus data with respect to binary-scaled pp collisions, with a hint of a larger suppression for the excited states [37–40]. These results also advocate for final-state effects at play in proton–nucleus collisions, such as those implemented in the comover models [36, 41] and/or the possible formation of a hot and dense medium (QGP) [42]. It is essential to perform precise measurements to elucidate and quantify the mechanisms at play.

Understanding the correlation between the soft and hard components of high-multiplicity events in small collision systems like pp is fundamental to disentangle initial and final-state effects affecting particle production, in particular in the heavy flavor sector. The ALICE collaboration has already contributed to these studies by measuring quarkonium and open heavy-flavor self-normalized yields as a function of the self-normalized charged-particle multiplicity density for center-of-mass energies of 5.02, 7 and 13 TeV [43–47]. The self-normalization is defined as the ratio of a given quantity to its average value: $dN_{ch}/d\eta / \langle dN_{ch}/d\eta \rangle$. Both the yields and the charged-particle multiplicity can be measured by ALICE

in the central and forward rapidity regions, leading to measurements with different kinematic configurations. In particular, one can choose to measure both quantities in approximately the same rapidity region, or to measure one at mid- and the other one at forward rapidity, introducing a gap in rapidity between the measurements of the quarkonium yield and of the charged-particle multiplicity density. In the charm sector, when the hard process is measured in the central rapidity region, a faster than linear increase with respect to the charged-particle multiplicity density is observed for D mesons [44] and J/ψ [45, 46], independently of the rapidity range of the multiplicity measurement. A qualitatively similar increase is also reported by the STAR collaboration for J/ψ in events reaching up to ~ 4 times the mean charged-particle multiplicity, in pp collisions at a lower energy ($\sqrt{s} = 200$ GeV), with the quarkonium yields and the charged-particle multiplicity measured in the same rapidity region [48]. In contrast, charmonium (J/ψ and $\psi(2S)$) yields at forward rapidity revealed an approximately linear increase of the yields with the charged-particle multiplicity density at midrapidity in pp data [43, 47, 49]. These results are described by several model calculations considering initial and final-state effects. The $\psi(2S)$ -to- J/ψ production ratio shows no significant multiplicity dependence when the multiplicity and charmonium yields are measured in the same rapidity range [47, 50]. Instead, a decreasing trend with multiplicity of the $\psi(2S)$ -to- J/ψ production ratio is observed when there is an overlap between the rapidity intervals in which the multiplicity and charmonium yields are measured [50].

In the beauty sector, the CMS collaboration investigated the event-activity dependence of $Y(nS)$ production at central rapidity in pp collisions at $\sqrt{s} = 2.76$ [51] and 7 TeV [52] and in p-Pb collisions at $\sqrt{s_{NN}} = 5.02$ TeV [51]. When the event activity is estimated in the range $|\eta^{\text{track}}| < 2.4$, a significant decrease of the excited-to-ground state ratios with increasing charged-particle multiplicity is reported, with no dependence on the azimuthal angle separation between the charged particles and the Y momentum direction. However, these ratios are found to be nearly independent of charged-particle multiplicity for jet-like events [52].

Measurements of bottomonium production at both central and forward rapidities in various collision systems are essential to better characterize the initial and final-state effects affecting particle production and their evolution with the charged-particle multiplicity density.

In this paper, the measurements of the $Y(1S)$, $Y(2S)$, and $Y(3S)$ yields, and excited-to-ground state ratios, performed with the ALICE detector, are reported as a function of charged-particle multiplicity density in pp collisions at $\sqrt{s} = 13$ TeV. $Y(nS)$ states are reconstructed in the dimuon decay channel at forward rapidity, whereas the charged-particle multiplicity density is measured at central rapidity. This configuration enables a gap in rapidity between the measurements of the Y yield and the charged-particle multiplicity density. To determine the charged-particle multiplicity density, the number of reconstructed tracklets is converted into a number of charged-particles by correcting for detector effects. This conversion procedure enables a direct comparison with theoretical calculations. Section 2 outlines the experimental apparatus and the data sample used in the analysis. Section 3 is devoted to the analysis. Section 4 presents and discusses the results in the current experimental and theoretical contexts. Finally, a summary and an outlook are given in Section 5.

2 Experimental apparatus and data sample

The ALICE apparatus is described in details in Refs. [53, 54]. This analysis exploits three detectors: the V0 for triggering and event selection; the Silicon Pixel Detector (SPD) for the measurement of the primary vertex position and the charged-particle multiplicity at central rapidity; the Muon Spectrometer (MS) for the measurement of the Y signal in the $\mu^+\mu^-$ decay channel at forward rapidity.

The V0 detector consists of two scintillator hodoscopes located on each side of the interaction point ($2.8 < \eta < 5.1$ and $-3.7 < \eta < -1.7$). It provides the minimum-bias (MB) trigger, requiring coincident signals in both hodoscopes. The SPD consists of two cylindrical layers, located at a radius $r = 3.9$ cm

and $r = 7.6$ cm from the beam axis, and covering the pseudorapidity ranges $|\eta| < 2$ and $|\eta| < 1.4$, respectively. The number of SPD tracklets (N_{trk}) is used for the estimation of the charged-particle multiplicity at central rapidity. Tracklets are defined as reconstructed line segments combining hits in the two SPD layers and pointing to the primary vertex. Muons originating from Y decays are detected in the MS, covering the pseudorapidity range $-4 < \eta < -2.5$. Starting from the interaction point, the MS is made of five tracking stations composed of two planes of cathode pad chambers, the third one installed within the gap of a dipole magnet providing a 3 T·m integrated magnetic field, and two trigger stations composed of two planes of resistive plate chambers. A front absorber of ~ 10 interaction lengths (λ_{int}) is placed between the interaction point and the first tracking station of the MS, to filter hadrons, which are further suppressed by a $7.2 \lambda_{\text{int}}$ thick iron wall installed between the tracking and trigger stations. A low-angle conical absorber shields the MS from the secondary particles produced by the interaction of primary particles with the beam pipe.

The results reported in this paper are obtained using the data collected in pp collisions at $\sqrt{s} = 13$ TeV, recorded by ALICE during the LHC Run 2. The charged-particle multiplicity is measured for events in the INEL >0 event class, which are defined as inelastic collisions for which at least one charged-particle track is detected in $|\eta| < 1$. The data used for the signal extraction were collected using a dimuon trigger, defined as the coincidence of a MB trigger and at least a pair of opposite-sign charge track segments reconstructed in the muon trigger system. The muon trigger system is configured to select muon tracks with a transverse momentum $p_{\text{T}}^{\mu} \gtrsim 0.5$ GeV/c. Because of the design of the muon trigger system, the selection on the muon transverse momentum does not correspond to a sharp threshold value. The reported value is the one for which the trigger efficiency is $\sim 50\%$. The number of MB- and dimuon-triggered events used for this analysis are about 125 millions and 367 millions, respectively. These correspond to an integrated luminosity of about 2 nb^{-1} and 16 pb^{-1} , respectively. At the maximum interaction rate, the probability of more than one pp collision occurring in the same bunch crossing was about 5×10^{-3} .

3 Analysis

The production of Y at forward rapidity ($2.5 < y < 4.0$) is studied as a function of the charged-particle multiplicity measured at central rapidity ($|\eta| < 1$). The Y yield (dN_{Y}/dy) and the pseudorapidity charged-particle multiplicity density ($dN_{\text{ch}}/d\eta$) are both measured for INEL >0 events.

Beam–gas events are rejected using timing cuts on the signals of the two V0 hodoscopes and the correlation between the number of clusters and track segments reconstructed in the SPD. Only events satisfying specific quality criteria for the primary vertex determination are selected. In particular, the precision of the vertex reconstructed with the SPD is required to be better than 0.25 cm along the z axis; the longitudinal interaction point position is required to be within $|z_{\text{vtx}}| < 10$ cm in order to minimize the variation of acceptance of the SPD when counting the tracklets in the region $|\eta| < 1$. Pileup in the SPD integration time ($\simeq 300$ ns) is reduced to a negligible contamination by removing events with multiple SPD vertices [43, 55].

The charged-particle multiplicity, $dN_{\text{ch}}/d\eta$, is estimated by counting the number of SPD tracklets in $|\eta| < 1$. To take into account the SPD acceptance variation with time and with the vertex position z_{vtx} in the data sample considered, a data-driven event-by-event correction method is applied, similar to the one described in Ref. [45]. This method consists in equalizing the measured $\langle N_{\text{trk}} \rangle(z_{\text{vtx}})$ profile to its maximum value ($\langle N_{\text{trk}} \rangle^{\text{max}} = 11.73$), where the correction term is smeared with a Poissonian distribution to mimic the event-by-event fluctuations. In the following, the tracklet multiplicity after the equalization procedure is referred to as the “corrected” tracklet multiplicity, $N_{\text{trk}}^{\text{corr}}$. In the analysis discussed in this paper, the events are grouped in $N_{\text{trk}}^{\text{corr}}$ classes: the resulting values of the self-normalized multiplicity for the considered event classes (where only events with $N_{\text{trk}}^{\text{corr}} > 1$ are used) are summarized in Table 1.

The production of secondary particles, either coming from the decay of primary particles or their inter-

Table 1: List of the event classes considered in the analysis, defined in terms of the $N_{\text{trk}}^{\text{corr}}$ measured in the SPD ($|\eta| < 1$). For each event class, the average self-normalized charged-particle multiplicity is indicated together with its systematic uncertainty (statistical uncertainties are negligible). The $N_{\text{trk}}^{\text{corr}}$ class interval 21 – 33 is only used for $\Upsilon(3S)$.

$N_{\text{trk}}^{\text{corr}}$	$\frac{dN_{\text{ch}}/d\eta}{\langle dN_{\text{ch}}/d\eta \rangle}$
1 – 8	0.38 ± 0.03
9 – 14	0.99 ± 0.02
15 – 20	1.51 ± 0.04
21 – 25	1.99 ± 0.04
21 – 33	2.24 ± 0.04
26 – 33	2.51 ± 0.04
34 – 41	3.16 ± 0.07
42 – 50	3.8 ± 0.1
51 – 60	4.5 ± 0.2
61 – 80	5.5 ± 0.3

action with the detector volumes, leads to a difference between the number of reconstructed tracklets and the number of primary charged particles N_{ch} [46]. Using Monte Carlo (MC) simulations based on the PYTHIA 8.2 [56] and EPOS-LHC [7] event generators, the correlation between $N_{\text{trk}}^{\text{corr}}$, and the number of generated primary charged particles N_{ch} is determined [46]. The propagation of the simulated particles in the detector apparatus is done with GEANT 3 [57], followed by the same reconstruction procedure as for data. An ad-hoc polynomial function f , described in appendix A, is used to parametrize the correlation between $N_{\text{trk}}^{\text{corr}}$ and N_{ch} in the full $N_{\text{trk}}^{\text{corr}}$ range. Finally, the self-normalized multiplicity is defined as the ratio of the average charged-particle multiplicity density in the analyzed multiplicity interval i , $dN_{\text{ch}}^i/d\eta$, to the average one:

$$\frac{dN_{\text{ch}}^i/d\eta}{\langle dN_{\text{ch}}/d\eta \rangle_{\text{INEL}>0}} = \frac{f(N_{\text{trk}}^{\text{corr}, i})}{\Delta\eta \times \langle dN_{\text{ch}}/d\eta \rangle_{\text{INEL}>0}}, \quad (1)$$

where $\Delta\eta = 2$ is the full pseudorapidity coverage considered for the measurement of the charged-particle multiplicity. The value of $\langle dN_{\text{ch}}/d\eta \rangle$, averaged over all events with $\text{INEL} > 0$, is measured as 7.02 ± 0.11 (syst.) for pp collisions at $\sqrt{s} = 13$ TeV [58].

The systematic uncertainty on the self-normalized charged-particle multiplicity $dN_{\text{ch}}^i/d\eta / \langle dN_{\text{ch}}/d\eta \rangle$ contains four contributions, detailed in Table 2: the calculation of $\langle N_{\text{ch}} \rangle$ for each multiplicity interval; the fitting functions used to parametrize the correlations between the tracklets and the charged-particle multiplicities, referred to as “ $N_{\text{trk}}^{\text{corr}}$ vs. N_{ch} non-linearity”; the charged-particle multiplicity averaged over all $\text{INEL} > 0$ events ($\langle dN_{\text{ch}}/d\eta \rangle$) and a correction to account for the MB trigger selection, affecting only the first multiplicity bin, $\epsilon_{\text{INEL}>0, \langle N_{\text{ch}} \rangle}^1$.

The systematic uncertainties for the calculation of the $\langle N_{\text{ch}} \rangle$ come from the residual dependence of $\langle N_{\text{ch}} \rangle$ on z_{vtx} , the dependence on the specific MC simulations, and the data-driven correction to the input profiles. The systematic uncertainty on the correlation encoded in the function f , introduced in Eq. 1, is estimated by varying the z_{vtx} range for the considered MC events ($[-10, -5]$, $[-5, 0]$, $[0, 5]$, $[5, 10]$ and $[-10, 10]$ cm ranges were considered) and the event generators (PYTHIA 8.2 (Monash 2013) and EPOS-LHC). The reference profile of the number of tracklets as a function of z_{vtx} is also varied in the equalization procedure, considering both the profile obtained from the data and the one from the MC (PYTHIA 8.2 or EPOS-LHC). The multiplicity $\langle N_{\text{ch}} \rangle$ is calculated as the average, and its systematic uncertainty as the standard deviation, of the distribution of the N_{ch} values obtained with the variations

described above. The resulting systematic uncertainty on $\langle N_{\text{ch}} \rangle$ ranges within 0.4–2%, depending on the multiplicity class.

The correlation between the tracklets and the charged-particle multiplicity is also studied replacing the polynomial approach described above with a linear fit function ($N_{\text{ch}} = \alpha \times N_{\text{trk}}^{\text{corr}}$), both globally (for the whole multiplicity range) and in the considered multiplicity intervals. The α factors and their uncertainties are computed by applying the same procedure as for the polynomial fit. In each multiplicity class, the difference originating from using either the global or the bin-by-bin α factor, and the two approaches for the fit function (linear and polynomial), is considered as an additional systematic uncertainty on the self-normalized multiplicity, “ $N_{\text{trk}}^{\text{corr}}$ vs N_{ch} non-linearity” in Table 2, amounting to 0–7%, depending on the multiplicity class.

$\langle dN_{\text{ch}}/d\eta \rangle_{\text{INEL}>0}$ represents the charged-particle multiplicity averaged over all INEL > 0 events. The value and its systematic uncertainty (1.6%) are taken from an independent analysis [58].

In addition, the lowest multiplicity class is affected by MB trigger selection, which removes very-low-multiplicity events. This effect is accounted for by dividing the $\langle N_{\text{ch}} \rangle$ value extracted for the first multiplicity interval by a correction factor $\epsilon_{\text{INEL}>0, \langle N_{\text{ch}} \rangle}^1$ (1.039), introducing an associated systematic uncertainty of 0.3%. The efficiency of the trigger selection, for any multiplicity class other than the lowest one is close to unity, and has negligible uncertainty. All the aforementioned systematic uncertainties are added in quadrature and summarized in Table 2. Whenever the source has a dependence on multiplicity, the minimum and maximum uncertainties are indicated.

Table 2: Summary of the systematic uncertainty sources in percentage on the self-normalized multiplicity. When the systematic uncertainty depends on the multiplicity class, the corresponding range is given. The quantity labelled with * is taken from an independent analysis [58]. All the mentioned systematic uncertainties are added in quadrature to the self-normalized multiplicity.

Source	%
$\langle N_{\text{ch}} \rangle$	0.4 – 2
$N_{\text{trk}}^{\text{corr}}$ vs. N_{ch} non-linearity	0 – 7
$\langle dN_{\text{ch}}/d\eta \rangle_{\text{INEL}>0}^*$	1.6
$\epsilon_{\text{INEL}>0, \langle N_{\text{ch}} \rangle}^1$	0.3
$dN_{\text{ch}}/d\eta / \langle dN_{\text{ch}}/d\eta \rangle_{\text{INEL}>0}$	1.7 – 7

The Y mesons are reconstructed in their dimuon decay channel. The muon track selection is identical to that used in Ref. [59]. The reconstructed dimuons are selected within the rapidity range $2.5 < y < 4.0$. The number of Y mesons is extracted from a log-likelihood binned fit to the invariant mass ($m_{\mu^+\mu^-}$) distribution. The fit is performed modeling the three Y(nS) peaks with a Double Crystal Ball (DCB) function each [60], and the underlying background with an ad hoc parametrization. Three functions are considered for the background, namely a variable-width Gaussian (VWG), a double-exponential function, and the product of an exponential and a power-law function, all described in appendix B. When fitting the multiplicity-integrated sample, the Y(1S) mass peak position and width are left free, while the DCB tail parameters are fixed to the values obtained from MC simulations.

The peak position and the width of the Y(2S) and Y(3S) signals are linked to the Y(1S) ones, through the ratio of the corresponding mass values taken from the Particle Data Group [61]. It was verified in Monte Carlo that the ratio of the Y(nS) states peak width values evolves as the ratio of the PDG peak mass values. The fit to the multiplicity-integrated sample is performed in three different mass ranges, namely [6, 13], [5, 14], and [7, 12] GeV/ c^2 , which results in nine different fit configurations. Due to the limited size of the available sample, in the individual multiplicity classes the Y(1S) peak position and width are fixed to the values obtained in the multiplicity-integrated sample, or to the same values varied by ± 1 sigma. Hence, for each combination of fit range and background function in the integrated sample, 81

different combinations of fit range, background function, Y(1S) mass, and Y(1S) width were tested, for each multiplicity class, resulting in 729 different fit configurations.

Considering the significance condition ($S/\sqrt{S+B} > 3$) for each Y state in the selected multiplicity class, the highest $N_{\text{trk}}^{\text{corr}}$ intervals in which the measurement is significant are [61, 80] for Y(1S) and Y(2S) and [21, 33] for Y(3S), corresponding to a self-normalized multiplicity of 5.5 ± 0.3 (syst.) and 2.24 ± 0.04 (syst.), respectively, as reported in Table 1. Figure 1 shows example fits to the dimuon invariant mass distributions for low- and high-multiplicity pp collisions.

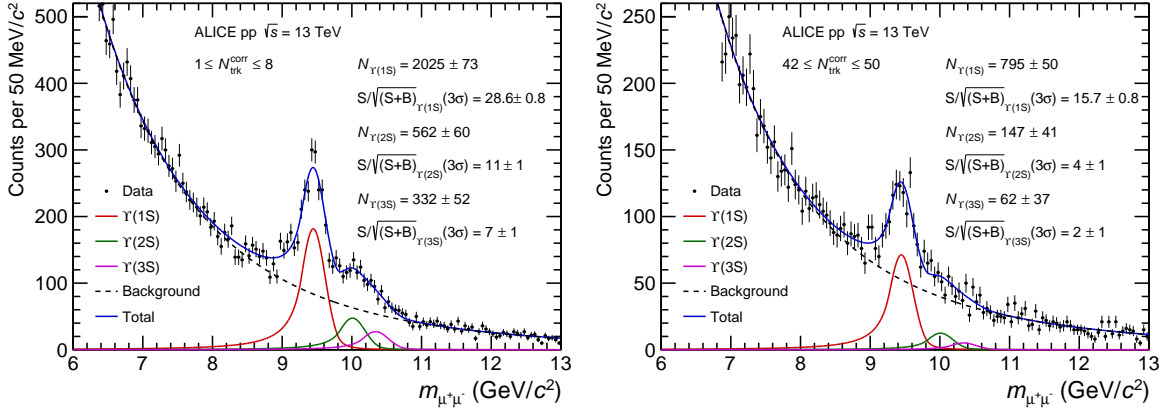


Figure 1: Dimuon invariant mass distribution for low-multiplicity pp collisions, corresponding to the $N_{\text{trk}}^{\text{corr}}$ interval bin [1, 8] (left) and for high-multiplicity pp collisions, corresponding to the $N_{\text{trk}}^{\text{corr}}$ interval bin [42, 50] (right). Significances ($S/\sqrt{S+B}$) are evaluated in a 3 standard deviation (3σ) window around the mean value of the peak.

The self-normalized yield of Y, i.e. the yield in a given multiplicity interval i normalized to the multiplicity-integrated value, is evaluated as

$$\frac{dN_Y^i/dy}{\langle dN_Y/dy \rangle} = \frac{N_Y^i}{N_Y} \times \frac{N_{\text{MB}}^{\text{eq}}}{N_{\text{MB}}^{\text{eq},i}} \times \frac{(A \times \varepsilon)_Y}{(A \times \varepsilon)_Y^i} \times \frac{\varepsilon_{\text{MB}}^i}{\varepsilon_{\text{MB}}} \times \frac{\varepsilon_Y}{\varepsilon_Y^i}, \quad (2)$$

where N_Y and $N_{\text{MB}}^{\text{eq}}$ are the number of reconstructed Y candidates and the equivalent number of MB events for the dimuon-triggered sample analyzed, respectively. The ratio $N_{\text{MB}}^{\text{eq},i}/N_{\text{MB}}^{\text{eq}}$ is the fraction of the MB cross section corresponding to multiplicity class i , and is calculated from the MB-triggered sample, as $N_{\text{MB}}^i/N_{\text{MB}}$.

The $A \times \varepsilon$ correction for N_Y is independent of multiplicity in the measured intervals, therefore, this factor cancels for the self-normalized yield measurement. The $1/\varepsilon_{\text{MB}}$ and $1/\varepsilon_Y$ represent correction factors applied on the number of MB selected events and number of reconstructed Y candidates, respectively, which are meant to account for the possible event and signal losses due to the event selections. These corrections include contributions from the efficiency of the MB trigger for events satisfying the $\text{INEL} > 0$ selection ($\varepsilon_{\text{INEL}>0, \text{yield}}^1$ and $\varepsilon_{\text{INEL}>0, \text{yield}}$), vertex quality selection ($\varepsilon_{\text{vtx, QA}}^{\text{Y(nS)}}$ and $\varepsilon_{\text{vtx, QA}}^{\text{MB}}$), and pileup rejection (ε_{pu}), same as in Ref. [43]. Finally, it is worth noting that the integrated number of MB events includes events with zero tracklets ($\text{INEL} = 0$ events): to remove this contamination, a specific correction factor ($\varepsilon_{\text{INEL}=0}$) is applied, as estimated from MC simulations. The values of all efficiency correction factors for the multiplicity-integrated case, as well as for the lowest multiplicity interval, are summarized in Table 3.

The systematic uncertainty on the Y signal extraction is estimated by varying the fit configuration as described above. The yield ratio N_Y^i/N_Y in multiplicity class i is computed for each of the 729 considered configurations, then the results are averaged and their *r.m.s.* is taken as the signal extraction systematic

Table 3: Summary of the efficiency factors which are applied to calculate the self-normalized yield of $\Upsilon(nS)$ along with their statistical uncertainties. The values quoted without uncertainty have negligible statistical uncertainty.

Efficiency	Value
$\epsilon_{\text{INEL}>0, \text{yield}}^1$	0.91
$\epsilon_{\text{INEL}>0, \text{yield}}$	0.95
$\epsilon_{\text{INEL}=0}$	0.98
$\epsilon_{\text{vtx, QA}}^{\text{MB}}$	0.94
$\epsilon_{\text{vtx, QA}}^{\Upsilon(1S)}$	0.97 ± 0.02
$\epsilon_{\text{vtx, QA}}^{\Upsilon(2S)}$	0.98 ± 0.06
$\epsilon_{\text{vtx, QA}}^{\Upsilon(3S)}$	0.95 ± 0.12

uncertainty. When double ratios are computed for the Υ measurement, the $\Upsilon(nS)/\Upsilon(1S)$ yield ratio is extracted for each fit configuration, then results are averaged and the *r.m.s.* taken as systematic uncertainty, so that correlated contributions to the signal extraction systematic uncertainty cancel. The uncertainty on the MB trigger efficiency ($\epsilon_{\text{INEL}>0, \text{yield}}$) is propagated to the Υ yields of the lowest and the integrated multiplicity classes, resulting in a systematic uncertainty of 1% ($\epsilon_{\text{INEL}>0, \text{yield}}^1$) and 0.5% ($\epsilon_{\text{INEL}>0, \text{yield}}$), respectively. The contamination efficiency factor $\epsilon_{\text{INEL}=0}$, mentioned before, is characterized by an associated systematic uncertainty of 2%, while the systematic uncertainty for the vertex quality correction and the pileup rejection (ϵ_{pu}) are both found to be negligible. As a further test, the ratio $N_{\text{MB}}^{\text{eq},i}/N_{\text{MB}}^{\text{eq}}$ is evaluated using the number of dimuon triggers and the trigger rejection factors in each multiplicity class, as detailed in Ref. [43], resulting in a negligible difference (0.02%) with respect to the approach considered in the present analysis.

All the aforementioned systematic uncertainties are added in quadrature and are reported in the bottom part of Table 4 as the total systematic uncertainty for each Υ state; whenever the source implies a dependence on multiplicity, the minimum and maximum uncertainties are indicated.

Table 4: Summary of the systematic uncertainties for the self-normalized Υ yields. The total systematic uncertainty for each self-normalized Υ state, shown in the bottom three lines, is computed as the quadratic sum of the contributions listed in the first part of the table. When the systematic uncertainty depends on the multiplicity class, the corresponding range is given.

Source	%
$\Upsilon(1S)$ signal extraction	1 – 6
$\Upsilon(2S)$ signal extraction	3 – 7
$\Upsilon(3S)$ signal extraction	7 – 13
$\epsilon_{\text{INEL}>0, \text{yield}}^1$	1
$\epsilon_{\text{INEL}>0, \text{yield}}$	0.5
$\epsilon_{\text{INEL}=0}$	2
$dN_{\Upsilon(1S)}/dy / \langle dN_{\Upsilon(1S)}/dy \rangle$	3 – 6
$dN_{\Upsilon(2S)}/dy / \langle dN_{\Upsilon(2S)}/dy \rangle$	4 – 7
$dN_{\Upsilon(3S)}/dy / \langle dN_{\Upsilon(3S)}/dy \rangle$	7 – 13

4 Results and discussion

The self-normalized yields, $dN_{\Upsilon}/dy / \langle dN_{\Upsilon}/dy \rangle$, as a function of the self-normalized charged-particle multiplicity density, $dN_{\text{ch}}/d\eta / \langle dN_{\text{ch}}/d\eta \rangle$, for the $\Upsilon(1S)$, $\Upsilon(2S)$, and $\Upsilon(3S)$ states, measured for $p_T > 0$, in pp collisions at $\sqrt{s} = 13$ TeV, are shown in Fig. 2. The bottom panel of Fig. 2 shows the double ratio of the self-normalized Υ yields to the self-normalized multiplicity. The self-normalized yields increase with the self-normalized charged-particle multiplicity. The scaling is compatible with a linear trend for

the three states. It results in a flat trend of the double ratios for the different states, within the uncertainties. The measurements are compared with the available theoretical models in Fig. 3. All calculations shown were performed in the same kinematic configuration as the measurement, for both the multiplicity and the $\Upsilon(nS)$ yields. At multiplicities up to 4 times the mean multiplicity, no relevant difference is observed between the PYTHIA 8.2 configurations, including feed-down from heavier states, with or without color reconnection (CR), which fairly describe the observed linear scaling. The implementation of the MPI mechanism corresponds to the simple scaling $N_{\text{MPI}} \propto N_{\text{hard process}} \propto N_{\text{ch}}$. The PYTHIA color reconnection scenario is a final-state effect at play with MPI, where strings are merged based on a QCD full color flow calculation with a loose modeling of dynamical effects via a global saturation [62]. CR is expected to have an impact both on the charged-particle multiplicity and the hard probe. At larger multiplicities, PYTHIA computations for the $\Upsilon(1S)$ deviate from the linear scaling, suggesting a weakening of the correlation. Computations from coherent particle production (CPP) [63] are also displayed: in this framework, high-multiplicity hadronic collisions are parameterized on equal footing regardless of the specific pp, p–A, or A–A system, allowing one to take into account features associated with nuclear effects. This is done by a phenomenological parametrization for mean multiplicities of light hadrons and quarkonia, assuming a linear dependence with the number of binary nucleon–nucleon interactions in p–A collisions. This model also takes into account the possible mutual boosting of the gluon densities and saturation scales in the colliding protons, induced by MPIs in a high-multiplicity environment, affecting the hard process (prompt production) [64]. The model is defined for $dN_{\text{ch}}/d\eta / \langle dN_{\text{ch}}/d\eta \rangle > 1$, corresponding to at least one nucleon–nucleon collision. Its uncertainties are inherited from the experimental uncertainties of the p–A measurements used to extract the model parameters. The CPP computations qualitatively describe the observed behavior within the current large theoretical and experimental uncertainties. In the computation with the CGC approach of Ref. [65], the probability to produce charmonia and bottomonia increases via a sizeable contribution of the multipomeron mechanism and especially the 3-pomeron term. It is enhanced, at high energy, thanks to additional t -channel gluons due to the increased gluon densities. The 3-pomeron CGC computation overestimates the measured dependence of $\Upsilon(1S)$ for the highest multiplicities reached, while no firm conclusion can be established for the excited states due to the large experimental uncertainties. It has to be noted that, despite the recent progress in the simultaneous computation or modelization of the soft and the hard components of hadronic interactions, there is a lack of predictions for bottomonia, except the PYTHIA 8.2, CPP and CGC in the 3-pomeron approach computations considered in this paper. Computations from CPP are not available for the $\Upsilon(3S)$ due to a lack of experimental measurements needed to extract the model parameters.

Figure 4 presents the Υ excited-to-ground state self-normalized yield ratios as a function of the self-normalized charged-particle multiplicity. A large fraction of the systematic uncertainties affecting the self-normalized yield of $\Upsilon(nS)$ states, dominated by signal extraction, cancels out in the excited-to-ground state ratios. The excited-to-ground state ratio of $\Upsilon(2S)$ to $\Upsilon(1S)$, shown in Fig. 4 (top panel), is compatible with unity within the uncertainties up to six times the mean charged-particle multiplicity. The measurement is compared with computations from PYTHIA 8.2, predicting a ratio close to unity at high multiplicity, independently of the considered color reconnection scenario, suggesting that final-state effects do not play a dominant role on the excited-to-ground Υ state yield ratio in pp collisions. The calculation from 3-pomeron CGC is also compatible with a ratio close to unity. A similar behavior can be observed in the CPP calculation, within large uncertainties. The measurement is also compared with computations from the comover model in which quarkonia are dissociated by interactions with final-state comoving particles [36, 41]. The dissociation rate is linked to the binding energy of the considered quarkonium state, and to the comover density. This last parameter also determines the uncertainties of the model. Feed-down contributions are taken into account in the computation. A decrease by 20% to 40% over the covered multiplicity range is predicted by this approach for the $\Upsilon(2S)$ -to- $\Upsilon(1S)$ ratio. It is worth noting that the CMS experiment reports a decrease of the $\Upsilon(2S)$ -to- $\Upsilon(1S)$ yield ratio as a function of the number of tracks when both quantities are measured in the central rapidity region in pp collisions

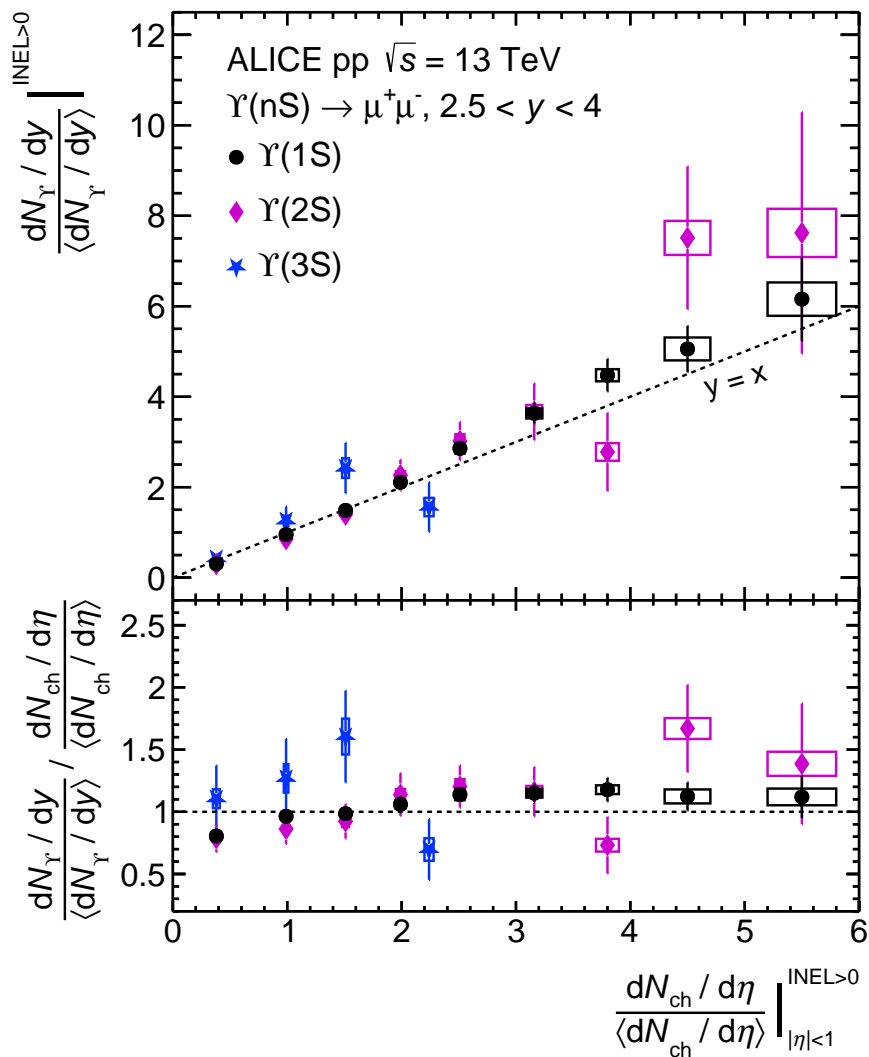


Figure 2: Self-normalized yield of $\Upsilon(nS)$ states as a function of self-normalized charged-particle multiplicity, p_T -integrated. The vertical error bars represent the statistical uncertainty on the Υ yields, while the systematic uncertainties on $dN_Y/dy / \langle dN_Y/dy \rangle$ and $dN_{ch}/d\eta / \langle dN_{ch}/d\eta \rangle$ are depicted as boxes. The dashed line shown in the top panel represents a linear function with the slope equal to unity.

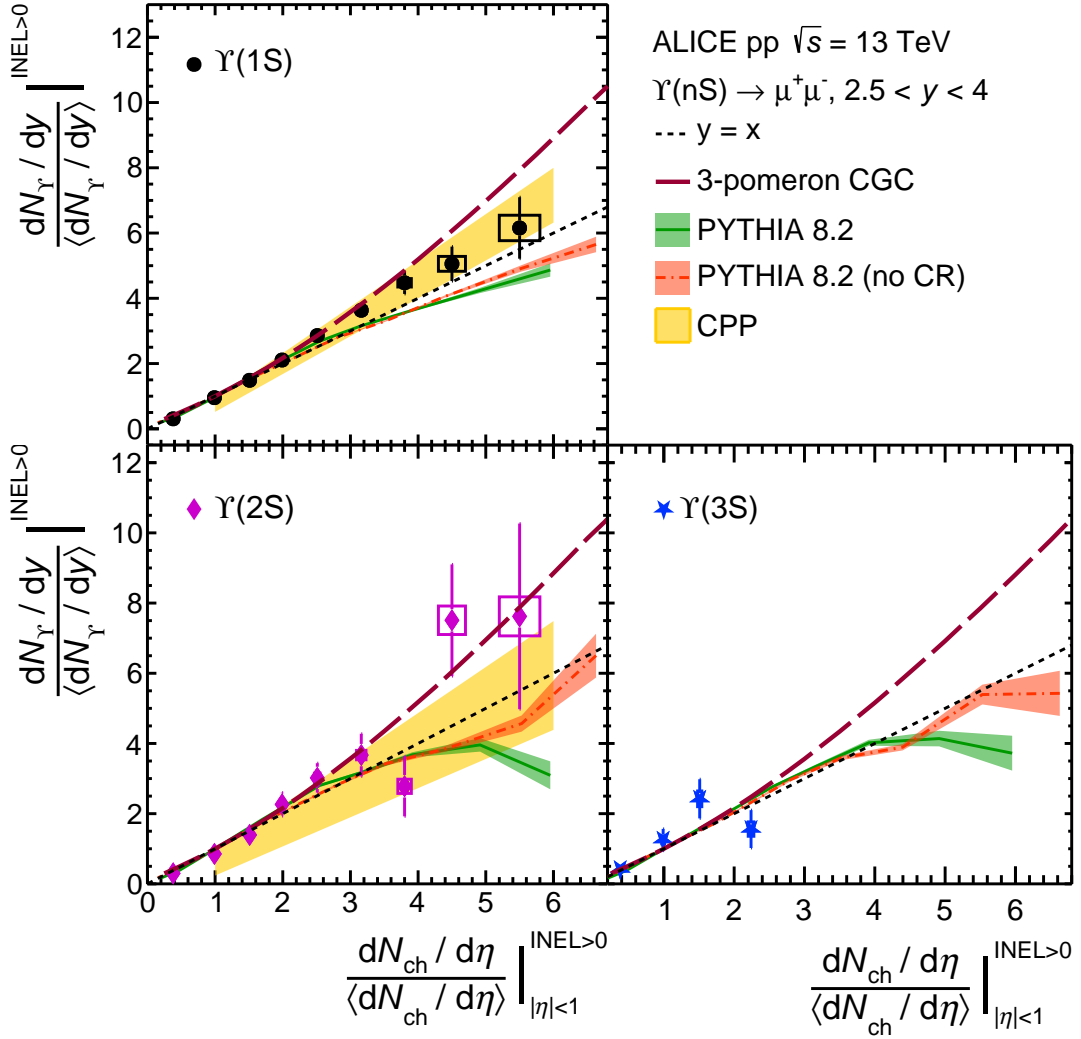


Figure 3: Self-normalized yield of $\Upsilon(nS)$ states as a function of self-normalized charged-particle multiplicity, p_T -integrated, compared to 3-pomeron CGC approach [65], PYTHIA 8.2 [5] and CPP [63]. The vertical error bars represent the statistical uncertainty, while the systematic uncertainties are depicted as boxes. The dashed line represents a linear function with the slope equal to unity.

at $\sqrt{s} = 2.76$ TeV [51] and 7 TeV [52]. On the contrary, when the measurement is performed with a gap in rapidity between the $\Upsilon(nS)$ states ($|y| < 1.93$) and the transverse energy measurement as an estimator of event activity ($|\eta| > 4$), a less pronounced decrease is observed in the ratio between the production yields of the two states [51]. The results presented in this paper are qualitatively compatible with the measurements reported by the CMS collaboration, regardless of whether these are given in terms of the forward or the midrapidity event activity. Figure 4 (bottom panel) shows the excited-to-ground state ratio of $\Upsilon(3S)$ -to- $\Upsilon(1S)$ yields. The measurement is compatible with unity within the large uncertainties, and with the almost flat trend predicted by PYTHIA 8.2, regardless of the considered color reconnection scenario, and by 3-pomeron CGC computations. It is interesting to note that, on the contrary, the comover scenario predicts a dissociation of $\Upsilon(3S)$ states leading to a large suppression at high charged-particle multiplicity (~ 6 times the mean multiplicity). For the $\Upsilon(2S)$ and $\Upsilon(3S)$ states, the discrepancy between data and the predictions of the comover model amounts to 1.8 and 1.7 sigmas, at most. Firm conclusions on the presence or absence of a final state Υ dissociation due to comoving particles would require further investigation based on larger data samples. These results convey a message consistent with the analogous measurements of the excited-to-ground state ratios in the charmonium sector [47, 50], described in the Introduction.

Figure 5 (top panel) presents the results discussed in this paper for the $\Upsilon(1S)$, $\Upsilon(2S)$, and $\Upsilon(3S)$, compared with analogous ALICE J/ψ measurements in the forward rapidity region at $\sqrt{s} = 5.02$ TeV [43], 7 TeV [45], and 13 TeV [43], exploiting the same multiplicity estimator as in the present analysis.

The $\Upsilon(1S)$ self-normalized production yield presents a similar scaling with the self-normalized charged-particle multiplicity density as the J/ψ , independently of the collision energy at which the J/ψ measurement is performed. This is further investigated, at $\sqrt{s} = 13$ TeV, in Fig. 5 (bottom panel), by presenting the double ratio of $\Upsilon(1S)$ -to- J/ψ self-normalized yields. The double ratio is close to unity for $dN_{ch}/d\eta / \langle dN_{ch}/d\eta \rangle > 1$, indicating no modification of the correlation with respect to mass and quark content up to six times the mean multiplicity. The ratio is also compared to the various available models, namely PYTHIA 8.2 with and without CR [5], the comover model [36, 41], the model by CPP [63], and the calculation of the 3-pomeron contribution in the CGC approach [65]. The considered models, except for 3-pomeron CGC, expect the double ratio to be close to unity over the whole charged-particle multiplicity range considered, suggesting that both initial and final-state effects act on $\Upsilon(1S)$ and J/ψ in a similar way. The first data point in Fig. 5 (bottom panel) is below unity by about two standard deviations. A possible mechanism explaining this behaviour invokes an event activity bias: events containing $\Upsilon(1S)$ are, on average, biased towards higher event activities than events containing J/ψ , and this behavior is expected to be driven by the mass difference of the two particles. The same mechanism could be expected when going from $\Upsilon(1S)$ to $\Upsilon(2S)$, and $\Upsilon(3S)$ states, currently not visible due to the relatively small mass difference between the three states, and the limited statistical significance of the higher-state measurements. In the 3-pomeron CGC computation, the increase of the $\Upsilon(1S)$ yield as a function of charged-particle multiplicity is expected to be faster than for J/ψ due to small mass-dependent higher twist effects, mainly visible at high multiplicities.

The results reported here for $\Upsilon(nS)$ yields in pp collisions at forward rapidity are consistent with published $\Upsilon(nS)$ measurements at central rapidity [51, 52]. These results follow a similar trend to that observed in analogous charmonium measurements [43, 45, 47, 50], within uncertainties.

5 Conclusions

The measurement of $\Upsilon(1S)$, $\Upsilon(2S)$, and $\Upsilon(3S)$ production as a function of the charged-particle multiplicity density in pp collisions at $\sqrt{s} = 13$ TeV, performed with the ALICE apparatus, is presented in this paper. The $\Upsilon(nS)$ states are measured in the dimuon decay channel in the forward rapidity region $2.5 < y < 4.0$, while the charged-particle multiplicity measurement is performed at central rapidity $|\eta| < 1$. In

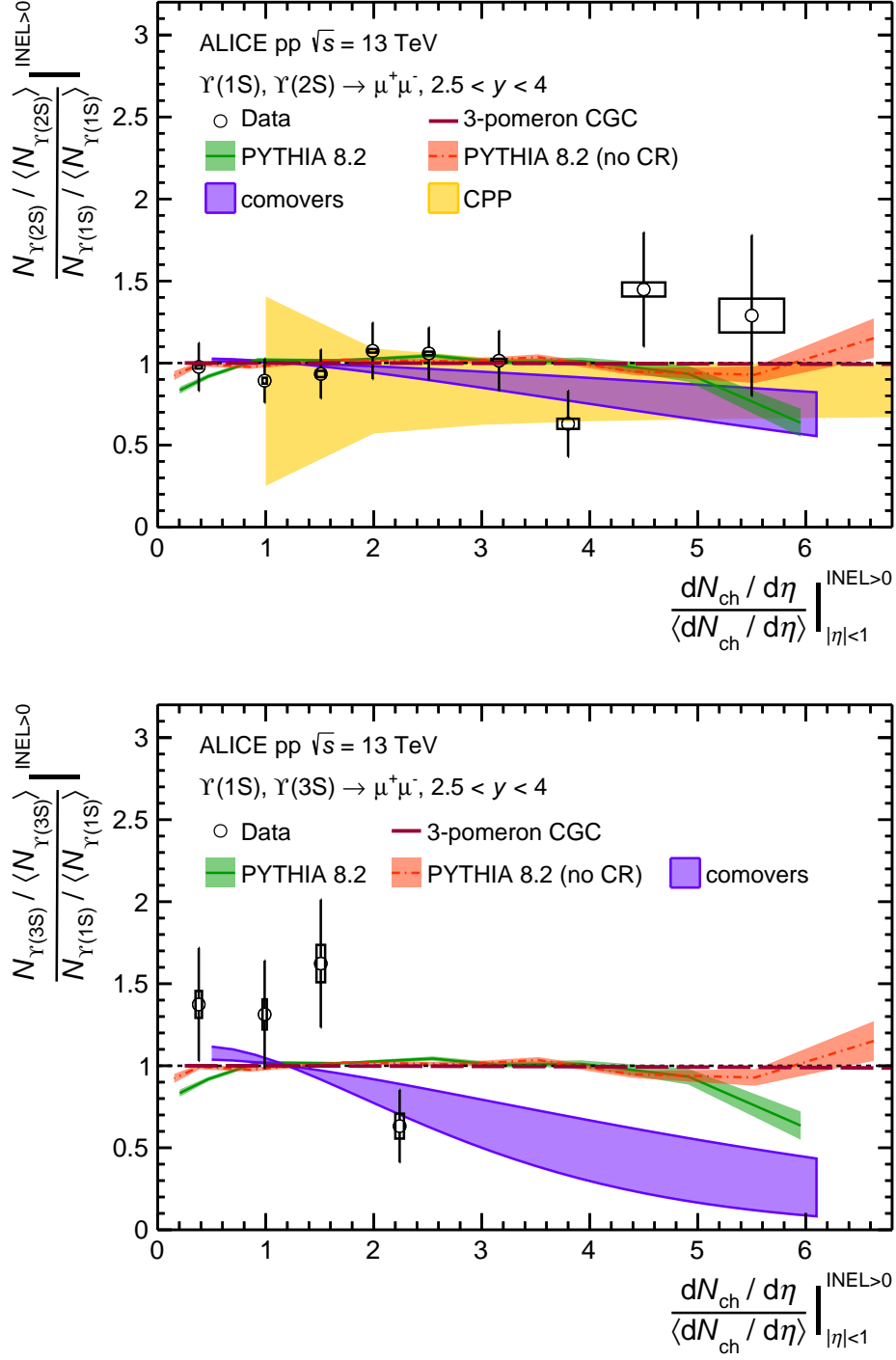


Figure 4: Top: Excited-to-ground state self-normalized yield ratio ($\Upsilon(2S)$ over $\Upsilon(1S)$) as a function of self-normalized charged-particle multiplicity, compared to model predictions from 3-pomeron CGC approach [65], PYTHIA 8.2 [5], comovers [36, 41], and CPP [63] calculations. Bottom: Excited-to-ground state self-normalized yield ratio ($\Upsilon(3S)$ over $\Upsilon(1S)$) as a function of self-normalized charged-particle multiplicity, compared to PYTHIA 8.2 and comovers predictions. The vertical error bars represent the statistical uncertainty, while the systematic uncertainties are depicted as boxes.

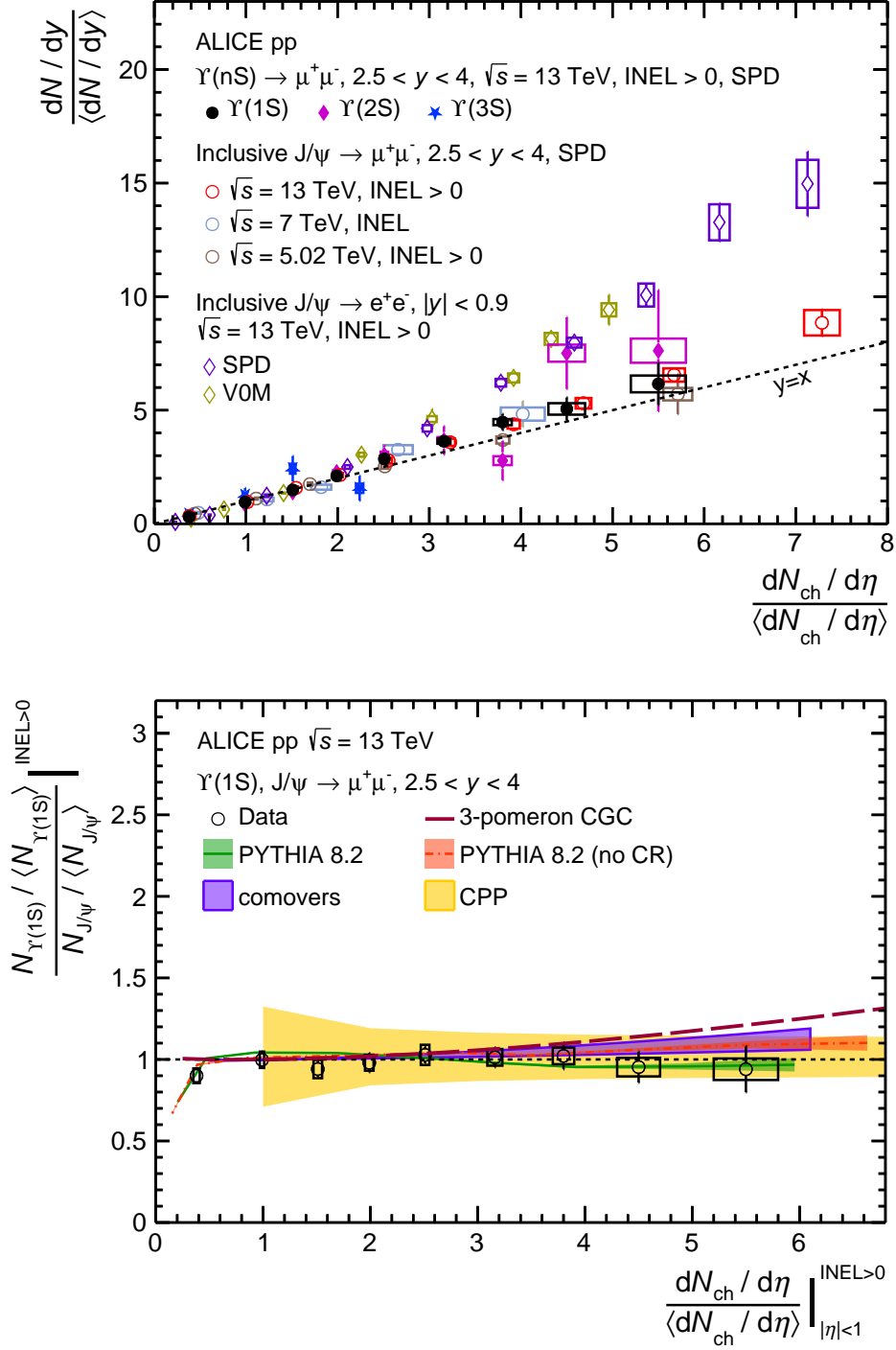


Figure 5: Top: Self-normalized yield of Υ as a function of self-normalized charged-particle multiplicity, compared to inclusive J/ψ measured in the forward rapidity region at $\sqrt{s} = 5.02$ TeV [43], 7 TeV [45], and 13 TeV [43], and to inclusive J/ψ measured in the central rapidity region at $\sqrt{s} = 13$ TeV [46]. Bottom: Self-normalized yield ratio of $\Upsilon(1S)$ -to- J/ψ as a function of self-normalized charged-particle multiplicity, compared to model computations from 3-pomeron CGC approach [65], PYTHIA 8.2 [5], comovers [36, 41], and CPP [63]. The vertical error bars represent the statistical uncertainty, while the systematic uncertainties on are depicted as boxes.

this rapidity configuration, the correlation between the self-normalized Y yields and the self-normalized charged-particle multiplicity density is compatible with a linear trend, with a slope consistent with unity within the uncertainties, in agreement with the expectations based on a naive MPI scenario. This behavior is qualitatively reproduced by PYTHIA 8.2 up to four times the mean multiplicity, regardless of the considered color reconnection scenario, as well as by computations from CPP and the 3-pomeron CGC approach.

The double ratios of the self-normalized yields of Y(2S) and Y(3S) to Y(1S) are compatible with unity in the explored multiplicity range within uncertainties, and in agreement with the predictions of PYTHIA 8.2, CPP and 3-pomeron CGC, as well as with the comover model calculations. With their current precision, these results can neither confirm nor exclude whether final-state effects are at play on Y(2S) and Y(3S) production at high multiplicity. The self-normalized double yield ratio of Y(1S)-to-J/ψ as a function of self-normalized charged-particle multiplicity is close to unity for $dN_{ch}/d\eta / \langle dN_{ch}/d\eta \rangle > 1$, and is described both by computations involving initial state effects (CPP and PYTHIA 8.2 without color reconnection), and final state effects, such as the comovers model and PYTHIA 8.2 calculations with color reconnection. The 3-pomeron CGC approach is disfavored.

The Y(nS) measurements reported here in pp collisions at forward rapidity are consistent with published Y(nS) results at central rapidity [51, 52]. These measurements follow the same pattern observed in the charmonium sector [43, 45, 47, 50], within uncertainties. Further measurements with the upgraded ALICE detector during the LHC Run 3 and Run 4 [66], allowing for an improved statistical precision of the measurements of excited bottomonium states, will be essential to elucidate and quantify possible final-state effects at play in the bottomonium sector.

Acknowledgements

We are very grateful to E. Ferreiro, B. Kopeliovich and M. Siddikov for sending us the calculations of their models and for fruitful discussions and clarifications about their computations. The ALICE Collaboration would like to thank all its engineers and technicians for their invaluable contributions to the construction of the experiment and the CERN accelerator teams for the outstanding performance of the LHC complex. The ALICE Collaboration gratefully acknowledges the resources and support provided by all Grid centres and the Worldwide LHC Computing Grid (WLCG) collaboration. The ALICE Collaboration acknowledges the following funding agencies for their support in building and running the ALICE detector: A. I. Alikhanyan National Science Laboratory (Yerevan Physics Institute) Foundation (ANSL), State Committee of Science and World Federation of Scientists (WFS), Armenia; Austrian Academy of Sciences, Austrian Science Fund (FWF): [M 2467-N36] and Nationalstiftung für Forschung, Technologie und Entwicklung, Austria; Ministry of Communications and High Technologies, National Nuclear Research Center, Azerbaijan; Conselho Nacional de Desenvolvimento Científico e Tecnológico (CNPq), Financiadora de Estudos e Projetos (Finep), Fundação de Amparo à Pesquisa do Estado de São Paulo (FAPESP) and Universidade Federal do Rio Grande do Sul (UFRGS), Brazil; Bulgarian Ministry of Education and Science, within the National Roadmap for Research Infrastructures 2020-2027 (object CERN), Bulgaria; Ministry of Education of China (MOEC), Ministry of Science & Technology of China (MSTC) and National Natural Science Foundation of China (NSFC), China; Ministry of Science and Education and Croatian Science Foundation, Croatia; Centro de Aplicaciones Tecnológicas y Desarrollo Nuclear (CEADEN), Cubaenergía, Cuba; Ministry of Education, Youth and Sports of the Czech Republic, Czech Republic; The Danish Council for Independent Research | Natural Sciences, the VILLUM FONDEN and Danish National Research Foundation (DNRF), Denmark; Helsinki Institute of Physics (HIP), Finland; Commissariat à l’Energie Atomique (CEA) and Institut National de Physique Nucléaire et de Physique des Particules (IN2P3) and Centre National de la Recherche Scientifique (CNRS), France; Bundesministerium für Bildung und Forschung (BMBF) and GSI Helmholtzzentrum für Schwerionenforschung GmbH, Germany; General Secretariat for Research and Technology, Ministry of Education,

Research and Religions, Greece; National Research, Development and Innovation Office, Hungary; Department of Atomic Energy Government of India (DAE), Department of Science and Technology, Government of India (DST), University Grants Commission, Government of India (UGC) and Council of Scientific and Industrial Research (CSIR), India; National Research and Innovation Agency - BRIN, Indonesia; Istituto Nazionale di Fisica Nucleare (INFN), Italy; Japanese Ministry of Education, Culture, Sports, Science and Technology (MEXT) and Japan Society for the Promotion of Science (JSPS) KAKENHI, Japan; Consejo Nacional de Ciencia (CONACYT) y Tecnología, through Fondo de Cooperación Internacional en Ciencia y Tecnología (FONCICYT) and Dirección General de Asuntos del Personal Académico (DGAPA), Mexico; Nederlandse Organisatie voor Wetenschappelijk Onderzoek (NWO), Netherlands; The Research Council of Norway, Norway; Commission on Science and Technology for Sustainable Development in the South (COMSATS), Pakistan; Pontificia Universidad Católica del Perú, Peru; Ministry of Education and Science, National Science Centre and WUT ID-UB, Poland; Korea Institute of Science and Technology Information and National Research Foundation of Korea (NRF), Republic of Korea; Ministry of Education and Scientific Research, Institute of Atomic Physics, Ministry of Research and Innovation and Institute of Atomic Physics and Universitatea Nationala de Stiinta si Tehnologie Politehnica Bucuresti, Romania; Ministry of Education, Science, Research and Sport of the Slovak Republic, Slovakia; National Research Foundation of South Africa, South Africa; Swedish Research Council (VR) and Knut & Alice Wallenberg Foundation (KAW), Sweden; European Organization for Nuclear Research, Switzerland; Suranaree University of Technology (SUT), National Science and Technology Development Agency (NSTDA) and National Science, Research and Innovation Fund (NSRF via PMU-B B05F650021), Thailand; Turkish Energy, Nuclear and Mineral Research Agency (TENMAK), Turkey; National Academy of Sciences of Ukraine, Ukraine; Science and Technology Facilities Council (STFC), United Kingdom; National Science Foundation of the United States of America (NSF) and United States Department of Energy, Office of Nuclear Physics (DOE NP), United States of America. In addition, individual groups or members have received support from: Marie Skłodowska Curie, European Research Council, Strong 2020 - Horizon 2020 (grant nos. 950692, 824093, 896850), European Union; Academy of Finland (Center of Excellence in Quark Matter) (grant nos. 346327, 346328), Finland; Programa de Apoyos para la Superación del Personal Académico, UNAM, Mexico.

References

- [1] Z. Citron *et al.*, “Future physics opportunities for high-density QCD at the LHC with heavy-ion and proton beams”, *CERN Yellow Rep. Monogr.* **7** (2019) 1159–1410, arXiv:1812.06772 [hep-ph].
- [2] C. Loizides, “Experimental overview on small collision systems at the LHC”, *Nucl. Phys. A* **956** (2016) 200–207, arXiv:1602.09138 [nucl-ex].
- [3] T. Sjöstrand and M. van Zijl, “A Multiple Interaction Model for the Event Structure in Hadron Collisions”, *Phys. Rev. D* **36** (1987) 2019.
- [4] ALICE Collaboration, J. Adam *et al.*, “Charged-particle multiplicities in proton–proton collisions at $\sqrt{s} = 0.9$ to 8 TeV”, *Eur. Phys. J. C* **77** (2017) 33, arXiv:1509.07541 [nucl-ex].
- [5] T. Sjöstrand, S. Mrenna and P. Z. Skands, “A Brief Introduction to PYTHIA 8.1”, *Comput. Phys. Commun.* **178** (2008) 852–867, arXiv:0710.3820 [hep-ph].
- [6] S. G. Weber, A. Dubla, A. Andronic, and A. Morsch, “Elucidating the multiplicity dependence of J/ψ production in proton–proton collisions with PYTHIA8”, *Eur. Phys. J. C* **79** (2019) 36, arXiv:1811.07744 [nucl-th].

- [7] T. Pierog, I. Karpenko, J. M. Katzy, E. Yatsenko, and K. Werner, “EPOS LHC: Test of collective hadronization with data measured at the CERN Large Hadron Collider”, *Phys. Rev. C* **92** (2015) 034906, arXiv:1306.0121 [hep-ph].
- [8] E. Cuautle, E. Dominguez, and I. Maldonado, “Extraction of multiple parton interactions and color reconnection from forward-backward multiplicity correlations”, *Eur. Phys. J. C* **79** (2019) 626, arXiv:1907.08706 [hep-ph].
- [9] J.-P. Lansberg, “New Observables in Inclusive Production of Quarkonia”, *Phys. Rept.* **889** (2020) 1–106, arXiv:1903.09185 [hep-ph].
- [10] A. Andronic *et al.*, “Heavy-flavour and quarkonium production in the LHC era: from proton–proton to heavy-ion collisions”, *Eur. Phys. J. C* **76** (2016) 107, arXiv:1506.03981 [nucl-ex].
- [11] S. Digal, P. Petreczky, and H. Satz, “Quarkonium feed down and sequential suppression”, *Phys. Rev. D* **64** (2001) 094015, arXiv:hep-ph/0106017.
- [12] B. Krouppa, R. Ryblewski, and M. Strickland, “Bottomonia suppression in 2.76 TeV Pb–Pb collisions”, *Phys. Rev. C* **92** (2015) 061901, arXiv:1507.03951 [hep-ph].
- [13] NA50 Collaboration, B. Alessandro *et al.*, “psi-prime production in Pb-Pb collisions at 158-GeV/nucleon”, *Eur. Phys. J. C* **49** (2007) 559–567, arXiv:nucl-ex/0612013.
- [14] PHENIX Collaboration, A. Adare *et al.*, “ J/ψ suppression at forward rapidity in Au+Au collisions at $\sqrt{s_{NN}} = 200$ GeV”, *Phys. Rev. C* **84** (2011) 054912, arXiv:1103.6269 [nucl-ex].
- [15] STAR Collaboration, J. Adam *et al.*, “Measurement of inclusive J/ψ suppression in Au+Au collisions at $\sqrt{s_{NN}} = 200$ GeV through the dimuon channel at STAR”, *Phys. Lett. B* **797** (2019) 134917, arXiv:1905.13669 [nucl-ex].
- [16] ALICE Collaboration, S. Acharya *et al.*, “Studies of J/ψ production at forward rapidity in Pb-Pb collisions at $\sqrt{s_{NN}} = 5.02$ TeV”, *JHEP* **02** (2020) 041, arXiv:1909.03158 [nucl-ex].
- [17] ALICE Collaboration, S. Acharya *et al.*, “ $\psi(2S)$ Suppression in Pb-Pb Collisions at the LHC”, *Phys. Rev. Lett.* **132** (2024) 042301, arXiv:2210.08893 [nucl-ex].
- [18] ATLAS Collaboration, M. Aaboud *et al.*, “Prompt and non-prompt J/ψ and $\psi(2S)$ suppression at high transverse momentum in 5.02 TeV Pb+Pb collisions with the ATLAS experiment”, *Eur. Phys. J. C* **78** (2018) 762, arXiv:1805.04077 [nucl-ex].
- [19] CMS Collaboration, A. M. Sirunyan *et al.*, “Measurement of prompt and nonprompt charmonium suppression in PbPb collisions at 5.02 TeV”, *Eur. Phys. J. C* **78** (2018) 509, arXiv:1712.08959 [nucl-ex]. [Erratum: *Eur.Phys.J.C* 83, 145 (2023)].
- [20] STAR Collaboration, B. Aboona *et al.*, “Observation of sequential Y suppression in Au+Au collisions at $\sqrt{s_{NN}} = 200$ GeV with the STAR experiment”, *Phys. Rev. Lett.* **130** (2023) 112301, arXiv:2207.06568 [nucl-ex].
- [21] PHENIX Collaboration, A. Adare *et al.*, “Measurement of $Y(1S + 2S + 3S)$ production in $p + p$ and Au+Au collisions at $\sqrt{s_{NN}} = 200$ GeV”, *Phys. Rev. C* **91** (2015) 024913, arXiv:1404.2246 [nucl-ex].
- [22] ATLAS Collaboration, G. Aad *et al.*, “Production of $Y(nS)$ mesons in Pb+Pb and pp collisions at 5.02 TeV”, *Phys. Rev. C* **107** (2023) 054912, arXiv:2205.03042 [nucl-ex].

- [23] **ALICE** Collaboration, S. Acharya *et al.*, “Y production and nuclear modification at forward rapidity in Pb–Pb collisions at $\sqrt{s_{NN}} = 5.02$ TeV”, *Phys. Lett. B* **822** (2021) 136579, arXiv:2011.05758 [nucl-ex].
- [24] **CMS** Collaboration, A. Tumasyan *et al.*, “Observation of the Y(3S) Meson and Suppression of Y(*n*S) States in PbPb Collisions at $\sqrt{s_{NN}} = 5.02$ TeV”, *Phys. Rev. Lett.* **133** (2024) 022302, arXiv:2303.17026 [hep-ex].
- [25] **STAR** Collaboration, M. Abdallah *et al.*, “Measurement of cold nuclear matter effects for inclusive J/ψ in p+Au collisions at sNN=200 GeV”, *Phys. Lett. B* **825** (2022) 136865, arXiv:2110.09666 [nucl-ex].
- [26] **LHCb** Collaboration, R. Aaij *et al.*, “Prompt and nonprompt J/ψ production and nuclear modification in pPb collisions at $\sqrt{s_{NN}} = 8.16$ TeV”, *Phys. Lett. B* **774** (2017) 159–178, arXiv:1706.07122 [hep-ex].
- [27] **ALICE** Collaboration, S. Acharya *et al.*, “Inclusive J/ψ production at forward and backward rapidity in p–Pb collisions at $\sqrt{s_{NN}} = 8.16$ TeV”, *JHEP* **07** (2018) 160, arXiv:1805.04381 [nucl-ex].
- [28] **ALICE** Collaboration, S. Acharya *et al.*, “J/ψ production at midrapidity in p–Pb collisions at $\sqrt{s_{NN}} = 8.16$ TeV”, *JHEP* **07** (2023) 137, arXiv:2211.14153 [nucl-ex].
- [29] **CMS** Collaboration, A. M. Sirunyan *et al.*, “Measurement of prompt and nonprompt J/ψ production in pp and pPb collisions at $\sqrt{s_{NN}} = 5.02$ TeV”, *Eur. Phys. J. C* **77** (2017) 269, arXiv:1702.01462 [nucl-ex].
- [30] **PHENIX** Collaboration, U. A. Acharya *et al.*, “Measurement of ψ(2S) nuclear modification at backward and forward rapidity in p + p, p + Al, and p + Au collisions at $\sqrt{s_{NN}} = 200$ GeV”, *Phys. Rev. C* **105** (2022) 064912, arXiv:2202.03863 [nucl-ex].
- [31] **LHCb** Collaboration, R. Aaij *et al.*, “Study of ψ(2S) production and cold nuclear matter effects in pPb collisions at $\sqrt{s_{NN}} = 5$ TeV”, *JHEP* **03** (2016) 133, arXiv:1601.07878 [nucl-ex].
- [32] **LHCb** Collaboration, R. Aaij *et al.*, “Prompt and nonprompt ψ(2S) production in pPb collisions at $\sqrt{s_{NN}} = 8.16$ TeV”, *JHEP* **04** (2024) 111, arXiv:2401.11342 [hep-ex].
- [33] **ALICE** Collaboration, J. Adam *et al.*, “Centrality dependence of ψ(2S) suppression in p–Pb collisions at $\sqrt{s_{NN}} = 5.02$ TeV”, *JHEP* **06** (2016) 050, arXiv:1603.02816 [nucl-ex].
- [34] **ALICE** Collaboration, S. Acharya *et al.*, “Centrality dependence of J/ψ and ψ(2S) production and nuclear modification in p–Pb collisions at $\sqrt{s_{NN}} = 8.16$ TeV”, *JHEP* **02** (2021) 002, arXiv:2008.04806 [nucl-ex].
- [35] **LHCb** Collaboration, R. Aaij *et al.*, “Charmonium production in pNe collisions at $\sqrt{s_{NN}} = 68.5$ GeV”, *Eur. Phys. J. C* **83** (2023) 625, arXiv:2211.11645 [hep-ex].
- [36] E. G. Ferreira, “Excited charmonium suppression in proton–nucleus collisions as a consequence of comovers”, *Phys. Lett. B* **749** (2015) 98–103, arXiv:1411.0549 [hep-ph].
- [37] **ALICE** Collaboration, S. Acharya *et al.*, “Y production in p–Pb collisions at $\sqrt{s_{NN}}=8.16$ TeV”, *Phys. Lett. B* **806** (2020) 135486, arXiv:1910.14405 [nucl-ex].
- [38] **ATLAS** Collaboration, M. Aaboud *et al.*, “Measurement of quarkonium production in proton–lead and proton–proton collisions at 5.02 TeV with the ATLAS detector”, *Eur. Phys. J. C* **78** (2018) 171, arXiv:1709.03089 [nucl-ex].

- [39] **CMS** Collaboration, A. Tumasyan *et al.*, “Nuclear modification of Y states in pPb collisions at $\sqrt{s_{NN}} = 5.02$ TeV”, *Phys. Lett. B* **835** (2022) 137397, arXiv:2202.11807 [hep-ex].
- [40] **LHCb** Collaboration, R. Aaij *et al.*, “Study of Y production in pPb collisions at $\sqrt{s_{NN}} = 8.16$ TeV”, *JHEP* **11** (2018) 194, arXiv:1810.07655 [hep-ex]. [Erratum: *JHEP* **02**, 093 (2020)].
- [41] A. Esposito, E. G. Ferreira, A. Pilloni, A. D. Polosa, and C. A. Salgado, “The nature of X(3872) from high-multiplicity pp collisions”, *Eur. Phys. J. C* **81** (2021) 669, arXiv:2006.15044 [hep-ph].
- [42] E. G. Ferreira and J.-P. Lansberg, “Is bottomonium suppression in proton-nucleus and nucleus-nucleus collisions at LHC energies due to the same effects?”, *JHEP* **10** (2018) 094, arXiv:1804.04474 [hep-ph]. [Erratum: *JHEP* **03**, 063 (2019)].
- [43] **ALICE** Collaboration, S. Acharya *et al.*, “Forward rapidity J/ψ production as a function of charged-particle multiplicity in pp collisions at $\sqrt{s} = 5.02$ and 13 TeV”, *JHEP* **06** (2022) 015, arXiv:2112.09433 [nucl-ex].
- [44] **ALICE** Collaboration, J. Adam *et al.*, “Measurement of charm and beauty production at central rapidity versus charged-particle multiplicity in proton-proton collisions at $\sqrt{s} = 7$ TeV”, *JHEP* **09** (2015) 148, arXiv:1505.00664 [nucl-ex].
- [45] **ALICE** Collaboration, B. Abelev *et al.*, “J/ψ Production as a Function of Charged Particle Multiplicity in pp Collisions at $\sqrt{s} = 7$ TeV”, *Phys. Lett. B* **712** (2012) 165–175, arXiv:1202.2816 [hep-ex].
- [46] **ALICE** Collaboration, S. Acharya *et al.*, “Multiplicity dependence of J/ψ production at midrapidity in pp collisions at $\sqrt{s} = 13$ TeV”, *Phys. Lett. B* **810** (2020) 135758, arXiv:2005.11123 [nucl-ex].
- [47] **ALICE** Collaboration, S. Acharya *et al.*, “Measurement of ψ(2S) production as a function of charged-particle pseudorapidity density in pp collisions at $\sqrt{s} = 13$ TeV and p-Pb collisions at $\sqrt{s_{NN}} = 8.16$ TeV with ALICE at the LHC”, *JHEP* **06** (2023) 147, arXiv:2204.10253 [nucl-ex].
- [48] **STAR** Collaboration, J. Adam *et al.*, “J/ψ production cross section and its dependence on charged-particle multiplicity in p + p collisions at $\sqrt{s} = 200$ GeV”, *Phys. Lett. B* **786** (2018) 87–93, arXiv:1805.03745 [hep-ex].
- [49] **ALICE** Collaboration, B. Abelev *et al.*, “J/ψ Production as a Function of Charged Particle Multiplicity in pp Collisions at $\sqrt{s} = 7$ TeV”, *Phys. Lett. B* **712** (2012) 165–175, arXiv:1202.2816 [hep-ex].
- [50] **LHCb** Collaboration, R. Aaij *et al.*, “Multiplicity dependence of $\sigma_{\psi(2S)}/\sigma_{J/\psi}$ in pp collisions at $\sqrt{s} = 13$ TeV”, *JHEP* **05** (2024) 243, arXiv:2312.15201 [hep-ex].
- [51] **CMS** Collaboration, S. Chatrchyan *et al.*, “Event Activity Dependence of Y(nS) Production in $\sqrt{s_{NN}} = 5.02$ TeV pPb and $\sqrt{s} = 2.76$ TeV pp Collisions”, *JHEP* **04** (2014) 103, arXiv:1312.6300 [nucl-ex].
- [52] **CMS** Collaboration, A. M. Sirunyan *et al.*, “Investigation into the event-activity dependence of Y(nS) relative production in proton-proton collisions at $\sqrt{s} = 7$ TeV”, *JHEP* **11** (2020) 001, arXiv:2007.04277 [hep-ex].
- [53] **ALICE** Collaboration, K. Aamodt *et al.*, “The ALICE experiment at the CERN LHC”, *JINST* **3** (2008) S08002.

- [54] **ALICE** Collaboration, B. Abelev *et al.*, “Performance of the ALICE experiment at the CERN LHC”, *Int. J. Mod. Phys. A* **29** (2014) 1430044, arXiv:1402.4476 [nucl-ex].
- [55] **ALICE** Collaboration, J. Adam *et al.*, “Charged-particle multiplicities in proton–proton collisions at $\sqrt{s} = 0.9$ to 8 TeV”, *Eur. Phys. J. C* **77** (2017) 33, arXiv:1509.07541 [nucl-ex].
- [56] T. Sjöstrand, S. Ask, J. R. Christiansen, R. Corke, N. Desai, P. Ilten, S. Mrenna, S. Prestel, C. O. Rasmussen, and P. Z. Skands, “An introduction to PYTHIA 8.2”, *Comput. Phys. Commun.* **191** (2015) 159–177, arXiv:1410.3012 [hep-ph].
- [57] R. Brun, F. Bruyant, F. Carminati, S. Giani, M. Maire, A. McPherson, G. Patrick, and L. Urban, *GEANT: Detector Description and Simulation Tool; Oct 1994*. CERN Program Library. CERN, Geneva, 1993. <https://cds.cern.ch/record/1082634>.
- [58] **ALICE** Collaboration, S. Acharya *et al.*, “Pseudorapidity distributions of charged particles as a function of mid- and forward rapidity multiplicities in pp collisions at $\sqrt{s} = 5.02, 7$ and 13 TeV”, *Eur. Phys. J. C* **81** (2021) 630, arXiv:2009.09434 [nucl-ex].
- [59] **ALICE** Collaboration, S. Acharya *et al.*, “Search for collectivity with azimuthal J/ψ-hadron correlations in high multiplicity p-Pb collisions at $\sqrt{s_{NN}} = 5.02$ and 8.16 TeV”, *Phys. Lett. B* **780** (2018) 7–20, arXiv:1709.06807 [nucl-ex].
- [60] **ALICE** Collaboration, S. Acharya *et al.*, “Measurement of Y(1S) elliptic flow at forward rapidity in Pb–Pb collisions at $\sqrt{s_{NN}} = 5.02$ TeV”, *Phys. Rev. Lett.* **123** (2019) 192301, arXiv:1907.03169 [nucl-ex].
- [61] **Particle Data Group** Collaboration, P. Zyla *et al.*, “Review of Particle Physics”, *PTEP* **2020** (2020) 083C01.
- [62] J. R. Christiansen and P. Z. Skands, “String Formation Beyond Leading Colour”, *JHEP* **08** (2015) 003, arXiv:1505.01681 [hep-ph].
- [63] B. Z. Kopeliovich, H. J. Pirner, I. K. Potashnikova, K. Reygers, and I. Schmidt, “Heavy quarkonium in the saturated environment of high-multiplicity pp collisions”, *Phys. Rev. D* **101** (2020) 054023, arXiv:1910.09682 [hep-ph].
- [64] B. Z. Kopeliovich, H. J. Pirner, I. K. Potashnikova, and I. Schmidt, “Mutual boosting of the saturation scales in colliding nuclei”, *Phys. Lett. B* **697** (2011) 333–338, arXiv:1007.1913 [hep-ph].
- [65] E. Levin, I. Schmidt, and M. Siddikov, “Multiplicity dependence of quarkonia production in the CGC approach”, *Eur. Phys. J. C* **80** (2020) 560, arXiv:1910.13579 [hep-ph].
- [66] **ALICE** Collaboration, S. Acharya *et al.*, “ALICE upgrades during the LHC Long Shutdown 2”, *JINST* **19** (2024) P05062, arXiv:2302.01238 [physics.ins-det].

A Polynomial function

An ad-hoc polynomial fitting function f is used to describe the relation between the number of SPD tracklets and charged-particle multiplicity, namely:

$$f(x) = ax^c + b \text{ for } x < x_0 \quad (\text{A.1})$$

$$f(x) = a_2x^{c_2} + b_2 \text{ for } x \geq x_0 \quad (\text{A.2})$$

where x_0 allow a better modeling of the shape with two different regions in x . x_0 is optimized by the fit and

$$a_2 = \left(\frac{ac}{c_2}\right)x_0^{c-c_2}, b_2 = \left(\frac{ac_2-ac}{c_2}\right)x_0^c + b$$

$$\langle N_{\text{ch}}^i \rangle = \frac{\sum N_j \times f(N_{\text{trk},j}^{\text{corr}})}{\sum N_j} \quad (\text{A.3})$$

where, N_j is the number of events in each $N_{\text{trk}}^{\text{corr}}$ bin taken from data.

B Background function

The Variable Width Gaussian (VWG) function is defined as

$$f(x; N, \bar{x}, A, B) = N \times \exp\left[-\frac{(x - \bar{x})^2}{2\sigma_{\text{VWG}}^2}\right] \quad (\text{B.1})$$

where,

$$\sigma_{\text{VWG}} = A + B \times \frac{x - \bar{x}}{\bar{x}}$$

A product of an exponential and a power-law function is defined as

$$f(x; p_0, p_1, p_2, p_3) = (p_1 + p_2x + p_3x^2)\exp(p_0x) \quad (\text{B.2})$$

A double exponential function is defined as














$$f(x; N_0, N_1, p_0, p_1) = N_0 \times \exp(p_0x) + N_1 \times \exp(p_1x) \quad (\text{B.3})$$

C The ALICE Collaboration

S. Acharya ¹²⁶, D. Adamová ⁸⁶, A. Adler⁷⁰, G. Aglieri Rinella ³², M. Agnello ²⁹, N. Agrawal ⁵¹, Z. Ahammed ¹³⁴, S. Ahmad ¹⁵, S.U. Ahn ⁷¹, I. Ahuja ³⁷, A. Akindinov ¹⁴⁰, M. Al-Turany ⁹⁸, D. Aleksandrov ¹⁴⁰, B. Alessandro ⁵⁶, H.M. Alfanda ⁶, R. Alfaro Molina ⁶⁷, B. Ali ¹⁵, Y. Ali¹³, A. Alici ²⁵, N. Alizadehvandchali ¹¹⁵, A. Alkin ³², J. Alme ²⁰, G. Alocco ⁵², T. Alt ⁶⁴, I. Altsybeev ¹⁴⁰, J.R. Alvarado ⁴⁴, M.N. Anaam ⁶, C. Andrei ⁴⁵, A. Andronic ¹²⁵, V. Anguelov ⁹⁵, F. Antinori ⁵⁴, P. Antonioli ⁵¹, C. Anuj ¹⁵, N. Apadula ⁷⁴, L. Aphecetche ¹⁰⁴, H. Appelshäuser ⁶⁴, C. Arata ⁷³, S. Arcelli ²⁵, M. Aresti ⁵², R. Arnaldi ⁵⁶, I.C. Arsene ¹⁹, M. Arslanok ¹³⁷, A. Augustinus ³², R. Averbeck ⁹⁸, M.D. Azmi ¹⁵, A. Badalà ⁵³, Y.W. Baek ⁴⁰, X. Bai ¹¹⁹, R. Bailhache ⁶⁴, Y. Bailung ⁴⁸, R. Bala ⁹¹, A. Balbino ²⁹, A. Baldisseri ¹²⁹, B. Balis ², D. Banerjee ⁴, Z. Banoo ⁹¹, R. Barbera ²⁶, F. Barile ³¹, L. Barioglio ⁹⁶, M. Barlou⁷⁸, G.G. Barnaföldi ⁴⁶, L.S. Barnby ⁸⁵, V. Barret ¹²⁶, L. Barreto ¹¹⁰, C. Bartels ¹¹⁸, K. Barth ³², E. Bartsch ⁶⁴, F. Baruffaldi ²⁷, N. Bastid ¹²⁶, S. Basu ⁷⁵, G. Batigne ¹⁰⁴, D. Battistini ⁹⁶, B. Batyunya ¹⁴¹, D. Bauri⁴⁷, J.L. Bazo Alba ¹⁰², I.G. Bearden ⁸³, C. Beattie ¹³⁷, P. Becht ⁹⁸, D. Behera ⁴⁸, I. Belikov ¹²⁸, A.D.C. Bell Hechavarria ¹²⁵, F. Bellini ²⁵, R. Bellwied ¹¹⁵, S. Belokurova ¹⁴⁰, V. Belyaev ¹⁴⁰, G. Bencedi ^{46,65}, S. Beole ²⁴, A. Bercuci ⁴⁵, Y. Berdnikov ¹⁴⁰, A. Berdnikova ⁹⁵, L. Bergmann ⁹⁵, M.G. Besoiu ⁶³, L. Betev ³², P.P. Bhaduri ¹³⁴, A. Bhasin ⁹¹, M.A. Bhat ⁴, B. Bhattacharjee ⁴¹, L. Bianchi ²⁴, N. Bianchi ⁴⁹, J. Bielčík ³⁵, J. Bielčíková ⁸⁶, J. Biernat ¹⁰⁷, A.P. Bigot ¹²⁸, A. Bilandzic ⁹⁶, G. Biro ⁴⁶, S. Biswas ⁴, N. Bize ¹⁰⁴, J.T. Blair ¹⁰⁸, D. Blau ¹⁴⁰, M.B. Blidaru ⁹⁸, N. Bluhme³⁸, C. Blume ⁶⁴, G. Boca ^{21,55}, F. Bock ⁸⁷, T. Bodova ²⁰, A. Bogdanov¹⁴⁰, S. Boi ²², J. Bok ⁵⁸, L. Boldizsár ⁴⁶, A. Bolozdynya ¹⁴⁰, M. Bombara ³⁷, P.M. Bond ³², G. Bonomi ^{133,55}, H. Borel ¹²⁹, A. Borissov ¹⁴⁰, A.G. Borquez Carcamo ⁹⁵, H. Bossi ¹³⁷, E. Botta ²⁴, Y.E.M. Bouziani ⁶⁴, L. Bratrud ⁶⁴, P. Braun-Munzinger ⁹⁸, M. Bregant ¹¹⁰, M. Broz ³⁵, G.E. Bruno ^{97,31}, M.D. Buckland ¹¹⁸, D. Budnikov ¹⁴⁰, H. Buesching ⁶⁴, S. Bufalino ²⁹, O. Bugnon¹⁰⁴, P. Buhler ¹⁰³, Z. Buthelezi ^{68,122}, J.B. Butt¹³, S.A. Bysiak¹⁰⁷, M. Cai ⁶, H. Caines ¹³⁷, A. Caliva ⁹⁸, E. Calvo Villar ¹⁰², J.M.M. Camacho ¹⁰⁹, P. Camerini ²³, F.D.M. Canedo ¹¹⁰, S.L. Cantway ¹³⁷, M. Carabas ¹¹³, A.A. Carballo ³², F. Carnesecchi ³², R. Caron ¹²⁷, J. Castillo Castellanos ¹²⁹, F. Catalano ^{24,29}, C. Ceballos Sanchez ¹⁴¹, I. Chakaberia ⁷⁴, P. Chakraborty ⁴⁷, S. Chandra ¹³⁴, S. Chapeland ³², M. Chartier ¹¹⁸, S. Chattopadhyay ¹³⁴, S. Chattopadhyay ¹⁰⁰, T. Cheng ^{98,6}, C. Cheshkov ¹²⁷, B. Cheynis ¹²⁷, V. Chibante Barroso ³², D.D. Chinellato ¹¹¹, E.S. Chizzali ^{11,96}, J. Cho ⁵⁸, S. Cho ⁵⁸, P. Chochula ³², P. Christakoglou ⁸⁴, C.H. Christensen ⁸³, P. Christiansen ⁷⁵, T. Chujo ¹²⁴, M. Ciaccio ²⁹, C. Cicalo ⁵², L. Cifarelli ²⁵, F. Cindolo ⁵¹, M.R. Ciupek⁹⁸, G. Clai^{III,51}, F. Colamaria ⁵⁰, J.S. Colburn¹⁰¹, D. Colella ^{97,31}, M. Colocci ³², M. Concas ⁵⁶, G. Conesa Balbastre ⁷³, Z. Conesa del Valle ¹³⁰, G. Contin ²³, J.G. Contreras ³⁵, M.L. Coquet ¹²⁹, T.M. Cormier^{I,87}, P. Cortese ^{132,56}, M.R. Cosentino ¹¹², F. Costa ³², S. Costanza ^{21,55}, J. Crkovská ⁹⁵, P. Crochet ¹²⁶, R. Cruz-Torres ⁷⁴, E. Cuautle⁶⁵, P. Cui ⁶, L. Cunqueiro⁸⁷, A. Dainese ⁵⁴, M.C. Danisch ⁹⁵, A. Danu ⁶³, P. Das ⁸⁰, P. Das ⁴, S. Das ⁴, A.R. Dash ¹²⁵, S. Dash ⁴⁷, A. De Caro ²⁸, G. de Cataldo ⁵⁰, J. de Cuveland³⁸, A. De Falco ²², D. De Gruttola ²⁸, N. De Marco ⁵⁶, C. De Martin ²³, S. De Pasquale ²⁸, S. Deb ⁴⁸, R.J. Debski ², K.R. Deja ¹³⁵, R. Del Grande ⁹⁶, L. Dello Stritto ²⁸, W. Deng ⁶, P. Dhankher ¹⁸, D. Di Bari ³¹, A. Di Mauro ³², R.A. Diaz ^{141,7}, T. Dietel ¹¹⁴, Y. Ding ^{127,6}, R. Divià ³², D.U. Dixit ¹⁸, Ø. Djuvsland²⁰, U. Dmitrieva ¹⁴⁰, A. Dobrin ⁶³, B. Dönigus ⁶⁴, A.K. Dubey ¹³⁴, J.M. Dubinski ¹³⁵, A. Dubla ⁹⁸, S. Dudi ⁹⁰, P. Dupieux ¹²⁶, M. Durkac ¹⁰⁶, N. Dzalaiova¹², T.M. Eder ¹²⁵, R.J. Ehlers ⁸⁷, V.N. Eikeland²⁰, F. Eisenhut ⁶⁴, D. Elia ⁵⁰, B. Erasmus ¹⁰⁴, F. Ercolessi ²⁵, F. Erhardt ⁸⁹, M.R. Ersdal²⁰, B. Espagnon ¹³⁰, G. Eulisse ³², D. Evans ¹⁰¹, S. Evdokimov ¹⁴⁰, L. Fabbietti ⁹⁶, M. Faggin ²⁷, J. Faivre ⁷³, F. Fan ⁶, W. Fan ⁷⁴, A. Fantoni ⁴⁹, M. Fasel ⁸⁷, P. Fedchio²⁹, A. Feliciello ⁵⁶, G. Feofilov ¹⁴⁰, A. Fernández Téllez ⁴⁴, M.B. Ferrer ³², A. Ferrero ¹²⁹, C. Ferrero ^{IV,56}, A. Ferretti ²⁴, V.J.G. Feuillard ⁹⁵, V. Filova ³⁵, D. Finogeev ¹⁴⁰, F.M. Fionda ⁵², F. Flor ¹¹⁵, A.N. Flores ¹⁰⁸, S. Foertsch ⁶⁸, I. Fokin ⁹⁵, S. Fokin ¹⁴⁰, E. Fragiocomo ⁵⁷, E. Frajna ⁴⁶, U. Fuchs ³², N. Funicello ²⁸, C. Furget ⁷³, A. Furs ¹⁴⁰, T. Fusayasu ⁹⁹, J.J. Gaardhøje ⁸³, M. Gagliardi ²⁴, A.M. Gago ¹⁰², C.D. Galvan ¹⁰⁹, D.R. Gangadharan ¹¹⁵, P. Ganoti ⁷⁸, C. Garabatos ⁹⁸, T. García Chávez ⁴⁴, E. Garcia-Solis ⁹, K. Garg ¹⁰⁴, C. Gargiulo ³², A. Garibli⁸¹, K. Garner¹²⁵, P. Gasik ⁹⁸, A. Gautam ¹¹⁷, M.B. Gay Ducati ⁶⁶, M. Germain ¹⁰⁴, C. Ghosh¹³⁴, S.K. Ghosh⁴, M. Giacalone ²⁵, P. Gianotti ⁴⁹, P. Giubellino ^{98,56}, P. Giubilato ²⁷, A.M.C. Glaenzer ¹²⁹, P. Glässel ⁹⁵, E. Glimos ¹²¹, D.J.Q. Goh⁷⁶, V. Gonzalez ¹³⁶, L.H. González-Trueba ⁶⁷, M. Gorgon ², S. Gotovac³³, V. Grabski ⁶⁷, L.K. Graczykowski ¹³⁵, E. Grecka ⁸⁶, A. Grelli ⁵⁹, C. Grigoras ³², V. Grigoriev ¹⁴⁰, S. Grigoryan ^{141,1}, F. Grosa ³², J.F. Grosse-Oetringhaus ³², R. Grosso ⁹⁸, D. Grund ³⁵, G.G. Guardiano ¹¹¹,

R. Guernane ⁷³, M. Guilbaud ¹⁰⁴, K. Gulbrandsen ⁸³, T. Gündem ⁶⁴, T. Gunji ¹²³, W. Guo ⁶,
A. Gupta ⁹¹, R. Gupta ⁹¹, L. Gyulai ⁴⁶, M.K. Habib ⁹⁸, C. Hadjidakis ¹³⁰, H. Hamagaki ⁷⁶,
A. Hamdi ⁷⁴, M. Hamid ⁶, Y. Han ¹³⁸, R. Hannigan ¹⁰⁸, M.R. Haque ¹³⁵, J.W. Harris ¹³⁷, A. Harton ⁹,
H. Hassan ⁸⁷, D. Hatzifotiadou ⁵¹, P. Hauer ⁴², L.B. Havener ¹³⁷, S.T. Heckel ⁹⁶, E. Hellbär ⁹⁸,
H. Helstrup ³⁴, M. Hemmer ⁶⁴, T. Herman ³⁵, G. Herrera Corral ⁸, F. Herrmann ¹²⁵, S. Herrmann ¹²⁷,
K.F. Hetland ³⁴, B. Heybeck ⁶⁴, H. Hillemanns ³², C. Hills ¹¹⁸, B. Hippolyte ¹²⁸, B. Hofman ⁵⁹,
B. Hohlweger ⁸⁴, J. Honermann ¹²⁵, G.H. Hong ¹³⁸, M. Horst ⁹⁶, A. Horzyk ², R. Hosokawa ¹⁴,
Y. Hou ⁶, P. Hristov ³², C. Hughes ¹²¹, P. Huhn ⁶⁴, L.M. Huhta ¹¹⁶, T.J. Humanic ⁸⁸, H. Hushnud ¹⁰⁰,
A. Hutson ¹¹⁵, D. Hutter ³⁸, J.P. Iddon ¹¹⁸, R. Ilkaev ¹⁴⁰, H. Ilyas ¹³, M. Inaba ¹²⁴, G.M. Innocenti ³²,
M. Ippolitov ¹⁴⁰, A. Isakov ⁸⁶, T. Isidori ¹¹⁷, M.S. Islam ¹⁰⁰, M. Ivanov ¹², M. Ivanov ⁹⁸, V. Ivanov ¹⁴⁰,
V. Izucheev ¹⁴⁰, M. Jablonski ², B. Jacak ⁷⁴, N. Jacazio ³², P.M. Jacobs ⁷⁴, S. Jadlovská ¹⁰⁶, J. Jadlovsky ¹⁰⁶,
S. Jaelani ⁸², L. Jaffe ³⁸, C. Jahnke ¹¹¹, M.J. Jakubowska ¹³⁵, M.A. Janik ¹³⁵, T. Janson ⁷⁰, M. Jercic ⁸⁹,
O. Jevons ¹⁰¹, A.A.P. Jimenez ⁶⁵, F. Jonas ^{87,125}, P.G. Jones ¹⁰¹, J.M. Jowett ^{32,98}, J. Jung ⁶⁴, M. Jung ⁶⁴,
A. Junique ³², A. Jusko ¹⁰¹, J. Kaewjai ¹⁰⁵, P. Kalinak ⁶⁰, A.S. Kalteyer ⁹⁸, A. Kalweit ³², V. Kaplin ¹⁴⁰,
A. Karasu Uysal ⁷², D. Karatovic ⁸⁹, O. Karavichev ¹⁴⁰, T. Karavicheva ¹⁴⁰, P. Karczmarczyk ¹³⁵,
E. Karpechev ¹⁴⁰, M.J. Karwowska ^{32,135}, V. Kashyap ⁸⁰, U. Keschull ⁷⁰, R. Keidel ¹³⁹,
D.L.D. Keijndener ⁵⁹, M. Keil ³², B. Ketzer ⁴², A.M. Khan ⁶, S. Khan ¹⁵, A. Khanzadeev ¹⁴⁰,
Y. Kharlov ¹⁴⁰, A. Khatun ¹⁵, A. Khuntia ¹⁰⁷, B. Kileng ³⁴, B. Kim ¹⁶, C. Kim ¹⁶, D.J. Kim ¹¹⁶,
E.J. Kim ⁶⁹, J. Kim ¹³⁸, J.S. Kim ⁴⁰, J. Kim ⁹⁵, J. Kim ⁶⁹, M. Kim ^{18,95}, S. Kim ¹⁷, T. Kim ¹³⁸,
K. Kimura ⁹³, S. Kirsch ⁶⁴, I. Kisel ³⁸, S. Kiselev ¹⁴⁰, A. Kisiel ¹³⁵, J.P. Kitowski ², J.L. Klay ⁵,
J. Klein ³², S. Klein ⁷⁴, C. Klein-Bösing ¹²⁵, M. Kleiner ⁶⁴, T. Klemenz ⁹⁶, A. Kluge ³²,
A.G. Knospe ¹¹⁵, C. Kobdaj ¹⁰⁵, T. Kollegger ⁹⁸, A. Kondratyev ¹⁴¹, E. Kondratyuk ¹⁴⁰, J. König ⁶⁴,
S.A. Königstorfer ⁹⁶, P.J. Konopka ³², G. Kornakov ¹³⁵, S.D. Koryciak ², A. Kotliarov ⁸⁶,
V. Kovalenko ¹⁴⁰, M. Kowalski ¹⁰⁷, V. Kozuharov ³⁶, I. Králik ⁶⁰, A. Kravčáková ³⁷, L. Kreis ⁹⁸,
M. Krivda ^{101,60}, F. Krizek ⁸⁶, K. Krizkova Gajdosova ³⁵, M. Kroesen ⁹⁵, M. Krüger ⁶⁴,
D.M. Krupova ³⁵, E. Kryshen ¹⁴⁰, V. Kučera ³², C. Kuhn ¹²⁸, P.G. Kuijer ⁸⁴, T. Kumaoka ¹²⁴,
D. Kumar ¹³⁴, L. Kumar ⁹⁰, N. Kumar ⁹⁰, S. Kumar ³¹, S. Kundu ³², P. Kurashvili ⁷⁹, A. Kurepin ¹⁴⁰,
A.B. Kurepin ¹⁴⁰, S. Kushpil ⁸⁶, J. Kvapil ¹⁰¹, M.J. Kweon ⁵⁸, J.Y. Kwon ⁵⁸, Y. Kwon ¹³⁸, S.L. La
Pointe ³⁸, P. La Rocca ²⁶, Y.S. Lai ⁷⁴, A. Lakrathok ¹⁰⁵, M. Lamanna ³², R. Langoy ¹²⁰, P. Larionov ³²,
E. Laudi ³², L. Lautner ^{32,96}, R. Lavicka ¹⁰³, T. Lazareva ¹⁴⁰, R. Lea ^{133,55}, G. Legras ¹²⁵,
J. Lehrbach ³⁸, R.C. Lemmon ⁸⁵, I. León Monzón ¹⁰⁹, M.M. Lesch ⁹⁶, E.D. Lesser ¹⁸, M. Lettrich ⁹⁶,
P. Lévai ⁴⁶, X. Li ¹⁰, X.L. Li ⁶, J. Lien ¹²⁰, R. Lietava ¹⁰¹, B. Lim ^{24,16}, S.H. Lim ¹⁶, V. Lindenstruth ³⁸,
A. Lindner ⁴⁵, C. Lippmann ⁹⁸, A. Liu ¹⁸, D.H. Liu ⁶, J. Liu ¹¹⁸, I.M. Lofnes ²⁰, C. Loizides ⁸⁷,
P. Loncar ³³, J.A. Lopez ⁹⁵, X. Lopez ¹²⁶, E. López Torres ⁷, P. Lu ^{98,119}, J.R. Luhder ¹²⁵,
M. Lunardon ²⁷, G. Luparello ⁵⁷, Y.G. Ma ³⁹, A. Maevskaya ¹⁴⁰, M. Mager ³², T. Mahmoud ⁴²,
A. Maire ¹²⁸, M.V. Makariev ³⁶, M. Malaev ¹⁴⁰, G. Malfattore ²⁵, N.M. Malik ⁹¹, Q.W. Malik ¹⁹,
S.K. Malik ⁹¹, L. Malinina ^{1, VIII, 141}, D. Mal'Kevich ¹⁴⁰, D. Mallick ⁸⁰, N. Mallick ⁴⁸,
G. Mandaglio ^{30,53}, V. Manko ¹⁴⁰, F. Manso ¹²⁶, V. Manzari ⁵⁰, Y. Mao ⁶, G.V. Margagliotti ²³,
A. Margotti ⁵¹, A. Marín ⁹⁸, C. Markert ¹⁰⁸, P. Martinengo ³², J.L. Martínez ¹¹⁵, M.I. Martínez ⁴⁴,
G. Martínez García ¹⁰⁴, S. Masciocchi ⁹⁸, M. Masera ²⁴, A. Masoni ⁵², L. Massacrier ¹³⁰,
A. Mastroserio ^{131,50}, A.M. Mathis ⁹⁶, O. Matonoha ⁷⁵, P.F.T. Matuoka ¹¹⁰, A. Matyja ¹⁰⁷, C. Mayer ¹⁰⁷,
A.L. Mazuecos ³², F. Mazzaschi ²⁴, M. Mazzilli ³², J.E. Mdhuli ¹²², A.F. Mechler ⁶⁴, Y. Melikyan ¹⁴⁰,
A. Menchaca-Rocha ⁶⁷, E. Meninno ¹⁰³, A.S. Menon ¹¹⁵, M. Meres ¹², S. Mhlanga ^{114,68}, Y. Miale ¹²⁴,
L. Micheletti ⁵⁶, L.C. Migliorin ¹²⁷, D.L. Mihaylov ⁹⁶, K. Mikhaylov ^{141,140}, A.N. Mishra ⁴⁶,
D. Miśkowiec ⁹⁸, A. Modak ⁴, A.P. Mohanty ⁵⁹, B. Mohanty ⁸⁰, M. Mohisin Khan ^{VI, 15},
M.A. Molander ⁴³, Z. Moravcova ⁸³, C. Mordasini ⁹⁶, D.A. Moreira De Godoy ¹²⁵, I. Morozov ¹⁴⁰,
A. Morsch ³², T. Mrnjavac ³², V. Muccifora ⁴⁹, S. Muhuri ¹³⁴, J.D. Mulligan ⁷⁴, A. Mulliri ²²,
M.G. Munhoz ¹¹⁰, R.H. Munzer ⁶⁴, H. Murakami ¹²³, S. Murray ¹¹⁴, L. Musa ³², J. Musinsky ⁶⁰,
J.W. Myrcha ¹³⁵, B. Naik ¹²², A.I. Nambrath ¹⁸, B.K. Nandi ⁴⁷, R. Nania ⁵¹, E. Nappi ⁵⁰,
A.F. Nassirpour ⁷⁵, A. Nath ⁹⁵, C. Nattrass ¹²¹, A. Neagu ¹⁹, A. Negru ¹¹³, L. Nellen ⁶⁵, S.V. Nesbo ³⁴,
G. Neskovic ³⁸, D. Nesterov ¹⁴⁰, B.S. Nielsen ⁸³, E.G. Nielsen ⁸³, S. Nikolaev ¹⁴⁰, S. Nikulin ¹⁴⁰,
V. Nikulin ¹⁴⁰, F. Noferini ⁵¹, S. Noh ¹¹, P. Nomokonov ¹⁴¹, J. Norman ¹¹⁸, N. Novitzky ¹²⁴,
P. Nowakowski ¹³⁵, A. Nyanin ¹⁴⁰, J. Nystrand ²⁰, M. Ogino ⁷⁶, A. Ohlson ⁷⁵, V.A. Okorokov ¹⁴⁰,
J. Olińczak ¹³⁵, A.C. Oliveira Da Silva ¹²¹, M.H. Oliver ¹³⁷, A. Onnerstad ¹¹⁶, C. Oppedisano ⁵⁶,
A. Ortiz Velasquez ⁶⁵, A. Oskarsson ⁷⁵, J. Otwinowski ¹⁰⁷, M. Oya ⁹³, K. Oyama ⁷⁶, Y. Pachmayer ⁹⁵,
S. Padhan ⁴⁷, D. Pagano ^{133,55}, G. Paic ⁶⁵, S. Paisano-Guzmán ⁴⁴, A. Palasciano ⁵⁰, S. Panebianco ¹²⁹,

H. Park ¹²⁴, J. Park ⁵⁸, J.E. Parkkila ³², R.N. Patra ⁹¹, B. Paul ²², H. Pei ⁶, T. Peitzmann ⁵⁹, X. Peng ⁶, M. Pennisi ²⁴, L.G. Pereira ⁶⁶, H. Pereira Da Costa ¹²⁹, D. Peresunko ¹⁴⁰, G.M. Perez ⁷, S. Perrin ¹²⁹, Y. Pestov ¹⁴⁰, V. Petráček ³⁵, V. Petrov ¹⁴⁰, M. Petrovici ⁴⁵, R.P. Pezzi ^{104,66}, S. Piano ⁵⁷, M. Pikna ¹², P. Pillot ¹⁰⁴, O. Pinazza ^{51,32}, L. Pinsky ¹¹⁵, C. Pinto ⁹⁶, S. Pisano ⁴⁹, M. Płoskoń ⁷⁴, M. Planinic ⁸⁹, F. Pliquett ⁶⁴, M.G. Poghosyan ⁸⁷, S. Politano ²⁹, N. Poljak ⁸⁹, A. Pop ⁴⁵, S. Porteboeuf-Houssais ¹²⁶, J. Porter ⁷⁴, V. Pozdniakov ^{1,141}, K.K. Pradhan ⁴⁸, S.K. Prasad ⁴, S. Prasad ⁴⁸, R. Preghenella ⁵¹, F. Prino ⁵⁶, C.A. Pruneau ¹³⁶, I. Pshenichnov ¹⁴⁰, M. Puccio ³², S. Pucillo ²⁴, Z. Pugelova ¹⁰⁶, S. Qiu ⁸⁴, L. Quaglia ²⁴, R.E. Quishpe ¹¹⁵, S. Ragoni ^{14,101}, A. Rakotozafindrabe ¹²⁹, L. Ramello ^{132,56}, F. Rami ¹²⁸, T.A. Rancien ⁷³, R. Raniwala ⁹², S. Raniwala ⁹², M. Rasa ²⁶, S.S. Räsänen ⁴³, R. Rath ^{51,48}, M.P. Rauch ²⁰, I. Ravasenga ⁸⁴, K.F. Read ^{87,121}, C. Reckziegel ¹¹², A.R. Redelbach ³⁸, K. Redlich ^{VII,79}, H.D. Regules-Medel ⁴⁴, A. Rehman ²⁰, F. Reidt ³², H.A. Reme-Ness ³⁴, Z. Rescakova ³⁷, K. Reyers ⁹⁵, A. Riabov ¹⁴⁰, V. Riabov ¹⁴⁰, R. Ricci ²⁸, T. Richert ⁷⁵, M. Richter ¹⁹, A.A. Riedel ⁹⁶, W. Riegler ³², F. Riggi ²⁶, C. Ristea ⁶³, M. Rodríguez Cahuantzi ⁴⁴, S.A. Rodríguez Ramírez ⁴⁴, K. Røed ¹⁹, R. Rogalev ¹⁴⁰, E. Rogochaya ¹⁴¹, T.S. Rogoschinski ⁶⁴, D. Rohr ³², D. Röhrich ²⁰, P.F. Rojas ⁴⁴, S. Rojas Torres ³⁵, P.S. Rokita ¹³⁵, G. Romanenko ¹⁴¹, F. Ronchetti ⁴⁹, A. Rosano ^{30,53}, E.D. Rosas ⁶⁵, A. Rossi ⁵⁴, A. Roy ⁴⁸, P. Roy ¹⁰⁰, S. Roy ⁴⁷, N. Rubini ²⁵, D. Ruggiano ¹³⁵, R. Rui ²³, B. Rumyantsev ¹⁴¹, P.G. Russek ², R. Russo ⁸⁴, A. Rustamov ⁸¹, E. Ryabinkin ¹⁴⁰, Y. Ryabov ¹⁴⁰, A. Rybicki ¹⁰⁷, H. Rytkonen ¹¹⁶, W. Rzesza ¹³⁵, O.A.M. Saarimaki ⁴³, R. Sadek ¹⁰⁴, S. Sadhu ³¹, S. Sadovsky ¹⁴⁰, J. Saetre ²⁰, K. Šafařík ³⁵, S.K. Saha ⁴, S. Saha ⁸⁰, B. Sahoo ⁴⁷, R. Sahoo ⁴⁸, S. Sahoo ⁶¹, D. Sahu ⁴⁸, P.K. Sahu ⁶¹, J. Saini ¹³⁴, K. Sajdakova ³⁷, S. Sakai ¹²⁴, M.P. Salvan ⁹⁸, S. Sambyal ⁹¹, I. Sanna ^{32,96}, T.B. Saramela ¹¹⁰, D. Sarkar ¹³⁶, N. Sarkar ¹³⁴, P. Sarma ⁴¹, V. Sarritzu ²², V.M. Sarti ⁹⁶, M.H.P. Sas ¹³⁷, J. Schambach ⁸⁷, H.S. Scheid ⁶⁴, C. Schiaua ⁴⁵, R. Schicker ⁹⁵, A. Schmah ⁹⁵, C. Schmidt ⁹⁸, H.R. Schmidt ⁹⁴, M.O. Schmidt ³², M. Schmidt ⁹⁴, N.V. Schmidt ⁸⁷, A.R. Schmier ¹²¹, R. Schotter ¹²⁸, J. Schukraft ³², K. Schwarz ⁹⁸, K. Schweda ⁹⁸, G. Scioli ²⁵, E. Scomparin ⁵⁶, J.E. Seger ¹⁴, Y. Sekiguchi ¹²³, D. Sekihata ¹²³, I. Selyuzhenkov ^{98,140}, S. Senyukov ¹²⁸, J.J. Seo ⁵⁸, D. Serebryakov ¹⁴⁰, L. Šerkšnytė ⁹⁶, A. Sevcenco ⁶³, T.J. Shaba ⁶⁸, A. Shabetai ¹⁰⁴, R. Shahoyan ³², A. Shangaraev ¹⁴⁰, A. Sharma ⁹⁰, D. Sharma ⁴⁷, H. Sharma ¹⁰⁷, M. Sharma ⁹¹, N. Sharma ⁹⁰, S. Sharma ⁷⁶, S. Sharma ⁹¹, U. Sharma ⁹¹, A. Shatat ¹³⁰, O. Sheibani ¹¹⁵, K. Shigaki ⁹³, M. Shimomura ⁷⁷, S. Shirinkin ¹⁴⁰, Q. Shou ³⁹, Y. Sibirjak ¹⁴⁰, S. Siddhanta ⁵², T. Siemiarzuk ⁷⁹, T.F. Silva ¹¹⁰, D. Silvermyr ⁷⁵, T. Simantathammakul ¹⁰⁵, R. Simeonov ³⁶, B. Singh ⁹¹, B. Singh ⁹⁶, R. Singh ⁸⁰, R. Singh ⁹¹, R. Singh ⁴⁸, S. Singh ¹⁵, V.K. Singh ¹³⁴, V. Singhal ¹³⁴, T. Sinha ¹⁰⁰, B. Sitar ¹², M. Sitta ^{132,56}, T.B. Skaali ¹⁹, G. Skorodumovs ⁹⁵, M. Slupecki ⁴³, N. Smirnov ¹³⁷, R.J.M. Snellings ⁵⁹, E.H. Solheim ¹⁹, J. Song ¹¹⁵, A. Songmoolnak ¹⁰⁵, F. Soramel ²⁷, R. Spijkers ⁸⁴, I. Sputowska ¹⁰⁷, J. Staa ⁷⁵, J. Stachel ⁹⁵, I. Stan ⁶³, P.J. Steffanic ¹²¹, S.F. Stiefelmaier ⁹⁵, D. Stocco ¹⁰⁴, I. Storehaug ¹⁹, M.M. Storetvedt ³⁴, P. Stratmann ¹²⁵, S. Strazzi ²⁵, C.P. Stylianidis ⁸⁴, A.A.P. Suaide ¹¹⁰, C. Suire ¹³⁰, M. Sukhanov ¹⁴⁰, M. Suljic ³², R. Sultanov ¹⁴⁰, V. Sumberia ⁹¹, S. Sumowidagdo ⁸², S. Swain ⁶¹, I. Szarka ¹², U. Tabassam ¹³, S.F. Taghavi ⁹⁶, G. Taillepiéd ⁹⁸, J. Takahashi ¹¹¹, G.J. Tambave ²⁰, S. Tang ^{126,6}, Z. Tang ¹¹⁹, J.D. Tapia Takaki ¹¹⁷, N. Tapus ¹¹³, L.A. Tarasovicova ¹²⁵, M.G. Tarzila ⁴⁵, G.F. Tassielli ³¹, A. Tauro ³², A. Telesca ³², L. Terlizzi ²⁴, C. Terrevoli ¹¹⁵, G. Tersimonov ³, S. Thakur ⁴, D. Thomas ¹⁰⁸, A. Tikhonov ¹⁴⁰, A.R. Timmins ¹¹⁵, M. Tkacik ¹⁰⁶, T. Tkacik ¹⁰⁶, A. Toia ⁶⁴, R. Tokumoto ⁹³, N. Topilskaya ¹⁴⁰, M. Toppi ⁴⁹, F. Torales-Acosta ¹⁸, T. Tork ¹³⁰, A.G. Torres Ramos ³¹, A. Trifiró ^{30,53}, A.S. Triolo ^{30,53}, S. Tripathy ⁵¹, T. Tripathy ⁴⁷, S. Trogolo ³², V. Trubnikov ³, W.H. Trzaska ¹¹⁶, T.P. Trzcinski ¹³⁵, R. Turrisi ⁵⁴, T.S. Tveter ¹⁹, K. Ullaland ²⁰, B. Ulukutlu ⁹⁶, A. Uras ¹²⁷, M. Urioni ^{55,133}, G.L. Usai ²², M. Vala ³⁷, N. Valle ²¹, S. Vallero ⁵⁶, L.V.R. van Doremalen ⁵⁹, C. Van Hulse ¹³⁰, M. van Leeuwen ⁸⁴, C.A. van Veen ⁹⁵, R.J.G. van Weelden ⁸⁴, P. Vande Vyvre ³², D. Varga ⁴⁶, Z. Varga ⁴⁶, M. Varga-Kofarago ⁴⁶, M. Vasileiou ⁷⁸, A. Vasiliev ¹⁴⁰, O. Vázquez Doce ⁴⁹, O. Vazquez Rueda ^{115,75}, V. Vechernin ¹⁴⁰, E. Vercellin ²⁴, S. Vergara Limón ⁴⁴, L. Vermunt ⁹⁸, R. Vértesi ⁴⁶, M. Verweij ⁵⁹, L. Vickovic ³³, Z. Vilakazi ¹²², O. Villalobos Baillie ¹⁰¹, G. Vino ⁵⁰, A. Vinogradov ¹⁴⁰, T. Virgili ²⁸, V. Vislavicius ⁸³, A. Vodopyanov ¹⁴¹, B. Volkel ³², M.A. Völkl ⁹⁵, K. Voloshin ¹⁴⁰, S.A. Voloshin ¹³⁶, G. Volpe ³¹, B. von Haller ³², I. Vorobyev ⁹⁶, N. Vozniuk ¹⁴⁰, J. Vrláková ³⁷, B. Wagner ²⁰, C. Wang ³⁹, D. Wang ³⁹, A. Wegrzynek ³², F.T. Weiglhofer ³⁸, S.C. Wenzel ³², J.P. Wessels ¹²⁵, J. Wiechula ⁶⁴, J. Wikne ¹⁹, G. Wilk ⁷⁹, J. Wilkinson ⁹⁸, G.A. Willems ¹²⁵, B. Windelband ⁹⁵, M. Winn ¹²⁹, J.R. Wright ¹⁰⁸, W. Wu ³⁹, Y. Wu ¹¹⁹, R. Xu ⁶, A. Yadav ⁴², A.K. Yadav ¹³⁴, S. Yalcin ⁷², Y. Yamaguchi ⁹³, K. Yamakawa ⁹³, S. Yang ²⁰, S. Yano ⁹³, Z. Yin ⁶, I.-K. Yoo ¹⁶, J.H. Yoon ⁵⁸, S. Yuan ²⁰, A. Yuncu ⁹⁵, V. Zaccolo ²³, C. Zampolli ³², H.J.C. Zanoli ⁵⁹, F. Zanone ⁹⁵, N. Zardoshti ^{32,101}, A. Zarochentsev ¹⁴⁰

P. Závada ⁶², N. Zaviyalov¹⁴⁰, M. Zhalov ¹⁴⁰, B. Zhang ⁶, S. Zhang ³⁹, X. Zhang ⁶, Y. Zhang¹¹⁹, Z. Zhang ⁶, M. Zhao ¹⁰, V. Zhrebchevskii ¹⁴⁰, Y. Zhi¹⁰, N. Zhigareva¹⁴⁰, D. Zhou ⁶, Y. Zhou ⁸³, J. Zhu ^{98,6}, Y. Zhu⁶, G. Zinovjev^{1,3}, S.C. Zugravel ⁵⁶, N. Zurlo ^{133,55}

Affiliation Notes

^I Deceased

^{II} Also at: Max-Planck-Institut für Physik, Munich, Germany

^{III} Also at: Italian National Agency for New Technologies, Energy and Sustainable Economic Development (ENEA), Bologna, Italy

^{IV} Also at: Dipartimento DET del Politecnico di Torino, Turin, Italy

^V Also at: Yildiz Technical University, Istanbul, Türkiye

^{VI} Also at: Department of Applied Physics, Aligarh Muslim University, Aligarh, India

^{VII} Also at: Institute of Theoretical Physics, University of Wrocław, Poland

^{VIII} Also at: An institution covered by a cooperation agreement with CERN

Collaboration Institutes

¹ A.I. Alikhanyan National Science Laboratory (Yerevan Physics Institute) Foundation, Yerevan, Armenia

² AGH University of Krakow, Cracow, Poland

³ Bogolyubov Institute for Theoretical Physics, National Academy of Sciences of Ukraine, Kiev, Ukraine

⁴ Bose Institute, Department of Physics and Centre for Astroparticle Physics and Space Science (CAPSS), Kolkata, India

⁵ California Polytechnic State University, San Luis Obispo, California, United States

⁶ Central China Normal University, Wuhan, China

⁷ Centro de Aplicaciones Tecnológicas y Desarrollo Nuclear (CEADEN), Havana, Cuba

⁸ Centro de Investigación y de Estudios Avanzados (CINVESTAV), Mexico City and Mérida, Mexico

⁹ Chicago State University, Chicago, Illinois, United States

¹⁰ China Institute of Atomic Energy, Beijing, China

¹¹ Chungbuk National University, Cheongju, Republic of Korea

¹² Comenius University Bratislava, Faculty of Mathematics, Physics and Informatics, Bratislava, Slovak Republic

¹³ COMSATS University Islamabad, Islamabad, Pakistan

¹⁴ Creighton University, Omaha, Nebraska, United States

¹⁵ Department of Physics, Aligarh Muslim University, Aligarh, India

¹⁶ Department of Physics, Pusan National University, Pusan, Republic of Korea

¹⁷ Department of Physics, Sejong University, Seoul, Republic of Korea

¹⁸ Department of Physics, University of California, Berkeley, California, United States

¹⁹ Department of Physics, University of Oslo, Oslo, Norway

²⁰ Department of Physics and Technology, University of Bergen, Bergen, Norway

²¹ Dipartimento di Fisica, Università di Pavia, Pavia, Italy

²² Dipartimento di Fisica dell'Università and Sezione INFN, Cagliari, Italy

²³ Dipartimento di Fisica dell'Università and Sezione INFN, Trieste, Italy

²⁴ Dipartimento di Fisica dell'Università and Sezione INFN, Turin, Italy

²⁵ Dipartimento di Fisica e Astronomia dell'Università and Sezione INFN, Bologna, Italy

²⁶ Dipartimento di Fisica e Astronomia dell'Università and Sezione INFN, Catania, Italy

²⁷ Dipartimento di Fisica e Astronomia dell'Università and Sezione INFN, Padova, Italy

²⁸ Dipartimento di Fisica 'E.R. Caianiello' dell'Università and Gruppo Collegato INFN, Salerno, Italy

²⁹ Dipartimento DISAT del Politecnico and Sezione INFN, Turin, Italy

³⁰ Dipartimento di Scienze MIFT, Università di Messina, Messina, Italy

³¹ Dipartimento Interateneo di Fisica 'M. Merlin' and Sezione INFN, Bari, Italy

³² European Organization for Nuclear Research (CERN), Geneva, Switzerland

³³ Faculty of Electrical Engineering, Mechanical Engineering and Naval Architecture, University of Split, Split, Croatia

³⁴ Faculty of Engineering and Science, Western Norway University of Applied Sciences, Bergen, Norway

³⁵ Faculty of Nuclear Sciences and Physical Engineering, Czech Technical University in Prague, Prague, Czech Republic

- ³⁶ Faculty of Physics, Sofia University, Sofia, Bulgaria
³⁷ Faculty of Science, P.J. Šafárik University, Košice, Slovak Republic
³⁸ Frankfurt Institute for Advanced Studies, Johann Wolfgang Goethe-Universität Frankfurt, Frankfurt, Germany
³⁹ Fudan University, Shanghai, China
⁴⁰ Gangneung-Wonju National University, Gangneung, Republic of Korea
⁴¹ Gauhati University, Department of Physics, Guwahati, India
⁴² Helmholtz-Institut für Strahlen- und Kernphysik, Rheinische Friedrich-Wilhelms-Universität Bonn, Bonn, Germany
⁴³ Helsinki Institute of Physics (HIP), Helsinki, Finland
⁴⁴ High Energy Physics Group, Universidad Autónoma de Puebla, Puebla, Mexico
⁴⁵ Horia Hulubei National Institute of Physics and Nuclear Engineering, Bucharest, Romania
⁴⁶ HUN-REN Wigner Research Centre for Physics, Budapest, Hungary
⁴⁷ Indian Institute of Technology Bombay (IIT), Mumbai, India
⁴⁸ Indian Institute of Technology Indore, Indore, India
⁴⁹ INFN, Laboratori Nazionali di Frascati, Frascati, Italy
⁵⁰ INFN, Sezione di Bari, Bari, Italy
⁵¹ INFN, Sezione di Bologna, Bologna, Italy
⁵² INFN, Sezione di Cagliari, Cagliari, Italy
⁵³ INFN, Sezione di Catania, Catania, Italy
⁵⁴ INFN, Sezione di Padova, Padova, Italy
⁵⁵ INFN, Sezione di Pavia, Pavia, Italy
⁵⁶ INFN, Sezione di Torino, Turin, Italy
⁵⁷ INFN, Sezione di Trieste, Trieste, Italy
⁵⁸ Inha University, Incheon, Republic of Korea
⁵⁹ Institute for Gravitational and Subatomic Physics (GRASP), Utrecht University/Nikhef, Utrecht, Netherlands
⁶⁰ Institute of Experimental Physics, Slovak Academy of Sciences, Košice, Slovak Republic
⁶¹ Institute of Physics, Homi Bhabha National Institute, Bhubaneswar, India
⁶² Institute of Physics of the Czech Academy of Sciences, Prague, Czech Republic
⁶³ Institute of Space Science (ISS), Bucharest, Romania
⁶⁴ Institut für Kernphysik, Johann Wolfgang Goethe-Universität Frankfurt, Frankfurt, Germany
⁶⁵ Instituto de Ciencias Nucleares, Universidad Nacional Autónoma de México, Mexico City, Mexico
⁶⁶ Instituto de Física, Universidade Federal do Rio Grande do Sul (UFRGS), Porto Alegre, Brazil
⁶⁷ Instituto de Física, Universidad Nacional Autónoma de México, Mexico City, Mexico
⁶⁸ iThemba LABS, National Research Foundation, Somerset West, South Africa
⁶⁹ Jeonbuk National University, Jeonju, Republic of Korea
⁷⁰ Johann-Wolfgang-Goethe Universität Frankfurt Institut für Informatik, Fachbereich Informatik und Mathematik, Frankfurt, Germany
⁷¹ Korea Institute of Science and Technology Information, Daejeon, Republic of Korea
⁷² KTO Karatay University, Konya, Turkey
⁷³ Laboratoire de Physique Subatomique et de Cosmologie, Université Grenoble-Alpes, CNRS-IN2P3, Grenoble, France
⁷⁴ Lawrence Berkeley National Laboratory, Berkeley, California, United States
⁷⁵ Lund University Department of Physics, Division of Particle Physics, Lund, Sweden
⁷⁶ Nagasaki Institute of Applied Science, Nagasaki, Japan
⁷⁷ Nara Women's University (NWU), Nara, Japan
⁷⁸ National and Kapodistrian University of Athens, School of Science, Department of Physics, Athens, Greece
⁷⁹ National Centre for Nuclear Research, Warsaw, Poland
⁸⁰ National Institute of Science Education and Research, Homi Bhabha National Institute, Jatni, India
⁸¹ National Nuclear Research Center, Baku, Azerbaijan
⁸² National Research and Innovation Agency - BRIN, Jakarta, Indonesia
⁸³ Niels Bohr Institute, University of Copenhagen, Copenhagen, Denmark
⁸⁴ Nikhef, National institute for subatomic physics, Amsterdam, Netherlands
⁸⁵ Nuclear Physics Group, STFC Daresbury Laboratory, Daresbury, United Kingdom
⁸⁶ Nuclear Physics Institute of the Czech Academy of Sciences, Husinec-Řež, Czech Republic
⁸⁷ Oak Ridge National Laboratory, Oak Ridge, Tennessee, United States
⁸⁸ Ohio State University, Columbus, Ohio, United States

- ⁸⁹ Physics department, Faculty of science, University of Zagreb, Zagreb, Croatia
- ⁹⁰ Physics Department, Panjab University, Chandigarh, India
- ⁹¹ Physics Department, University of Jammu, Jammu, India
- ⁹² Physics Department, University of Rajasthan, Jaipur, India
- ⁹³ Physics Program and International Institute for Sustainability with Knotted Chiral Meta Matter (SKCM2), Hiroshima University, Hiroshima, Japan
- ⁹⁴ Physikalisches Institut, Eberhard-Karls-Universität Tübingen, Tübingen, Germany
- ⁹⁵ Physikalisches Institut, Ruprecht-Karls-Universität Heidelberg, Heidelberg, Germany
- ⁹⁶ Physik Department, Technische Universität München, Munich, Germany
- ⁹⁷ Politecnico di Bari and Sezione INFN, Bari, Italy
- ⁹⁸ Research Division and ExtreMe Matter Institute EMMI, GSI Helmholtzzentrum für Schwerionenforschung GmbH, Darmstadt, Germany
- ⁹⁹ Saga University, Saga, Japan
- ¹⁰⁰ Saha Institute of Nuclear Physics, Homi Bhabha National Institute, Kolkata, India
- ¹⁰¹ School of Physics and Astronomy, University of Birmingham, Birmingham, United Kingdom
- ¹⁰² Sección Física, Departamento de Ciencias, Pontificia Universidad Católica del Perú, Lima, Peru
- ¹⁰³ Stefan Meyer Institut für Subatomare Physik (SMI), Vienna, Austria
- ¹⁰⁴ SUBATECH, IMT Atlantique, Nantes Université, CNRS-IN2P3, Nantes, France
- ¹⁰⁵ Suranaree University of Technology, Nakhon Ratchasima, Thailand
- ¹⁰⁶ Technical University of Košice, Košice, Slovak Republic
- ¹⁰⁷ The Henryk Niewodniczanski Institute of Nuclear Physics, Polish Academy of Sciences, Cracow, Poland
- ¹⁰⁸ The University of Texas at Austin, Austin, Texas, United States
- ¹⁰⁹ Universidad Autónoma de Sinaloa, Culiacán, Mexico
- ¹¹⁰ Universidade de São Paulo (USP), São Paulo, Brazil
- ¹¹¹ Universidade Estadual de Campinas (UNICAMP), Campinas, Brazil
- ¹¹² Universidade Federal do ABC, Santo Andre, Brazil
- ¹¹³ Universitatea Nationala de Stiinta si Tehnologie Politehnica Bucuresti, Bucharest, Romania
- ¹¹⁴ University of Cape Town, Cape Town, South Africa
- ¹¹⁵ University of Houston, Houston, Texas, United States
- ¹¹⁶ University of Jyväskylä, Jyväskylä, Finland
- ¹¹⁷ University of Kansas, Lawrence, Kansas, United States
- ¹¹⁸ University of Liverpool, Liverpool, United Kingdom
- ¹¹⁹ University of Science and Technology of China, Hefei, China
- ¹²⁰ University of South-Eastern Norway, Kongsberg, Norway
- ¹²¹ University of Tennessee, Knoxville, Tennessee, United States
- ¹²² University of the Witwatersrand, Johannesburg, South Africa
- ¹²³ University of Tokyo, Tokyo, Japan
- ¹²⁴ University of Tsukuba, Tsukuba, Japan
- ¹²⁵ Universität Münster, Institut für Kernphysik, Münster, Germany
- ¹²⁶ Université Clermont Auvergne, CNRS/IN2P3, LPC, Clermont-Ferrand, France
- ¹²⁷ Université de Lyon, CNRS/IN2P3, Institut de Physique des 2 Infinis de Lyon, Lyon, France
- ¹²⁸ Université de Strasbourg, CNRS, IPHC UMR 7178, F-67000 Strasbourg, France, Strasbourg, France
- ¹²⁹ Université Paris-Saclay, Centre d'Etudes de Saclay (CEA), IRFU, Département de Physique Nucléaire (DPhN), Saclay, France
- ¹³⁰ Université Paris-Saclay, CNRS/IN2P3, IJCLab, Orsay, France
- ¹³¹ Università degli Studi di Foggia, Foggia, Italy
- ¹³² Università del Piemonte Orientale, Vercelli, Italy
- ¹³³ Università di Brescia, Brescia, Italy
- ¹³⁴ Variable Energy Cyclotron Centre, Homi Bhabha National Institute, Kolkata, India
- ¹³⁵ Warsaw University of Technology, Warsaw, Poland
- ¹³⁶ Wayne State University, Detroit, Michigan, United States
- ¹³⁷ Yale University, New Haven, Connecticut, United States
- ¹³⁸ Yonsei University, Seoul, Republic of Korea
- ¹³⁹ Zentrum für Technologie und Transfer (ZTT), Worms, Germany
- ¹⁴⁰ Affiliated with an institute covered by a cooperation agreement with CERN
- ¹⁴¹ Affiliated with an international laboratory covered by a cooperation agreement with CERN.